Journal of Theoretical Biology 595 (2024) 111934

Contents lists available at ScienceDirect

Journal of Theoretical Biology

journal homepage: www.elsevier.com/locate/yjtbi

An approximate solution of the SLIP model under the regime of linear angular dynamics during stance and the stability of symmetric periodic running gaits

Alessandro Maria Selvitella [a,b,c,*], Kathleen Lois Foster [d,c]

[a] Department of Mathematical Sciences, Purdue University Fort Wayne, 2101 E Coliseum Blvd, Fort Wayne, IN, 46805, United States of America
[b] eScience Institute, University of Washington, 3910 15th Ave NE, Seattle, WA 98195, United States of America
[c] NSF-Simons Center for Quantitative Biology, Northwestern University, 2200 Campus Drive, Evanston, IL 60208, United States of America
[d] Department of Biology, Ball State University, 2000 W University Ave, Muncie, IN 47306, United States of America

ARTICLE INFO

Keywords:
SLIP dynamics
Hybrid dynamical systems
Poincare' map
Stability of periodic solutions
Human running
Gait stability

ABSTRACT

Terrestrial locomotion is a complex phenomenon that is often linked to the survival of an individual and of an animal species. Mathematical models seek to express in quantitative terms how animals move, but this is challenging because the ways in which the nervous and musculoskeletal systems interact to produce body movement is not completely understood. Models with many variables tend to lack biological interpretability and describe the motion of an animal with too many independent degrees of freedom. Instead, reductionist models aim to describe the essential features of a gait with the smallest number of variables, often concentrating on the center of mass dynamics. In particular, spring–mass models have been successful in extracting and describing important characteristics of running. In this paper, we consider the spring loaded inverted pendulum model under the regime of constant angular velocity, small compression, and small angle swept during stance. We provide conditions for the asymptotic stability of periodic trajectories for the full range of parameters. The hypothesis of linear angular dynamics during stance is successfully tested on publicly available human data of individuals running on a treadmill at different velocities. Our analysis highlights a novel bifurcation phenomenon for varying *Froude number*: there are periodic trajectories of the spring loaded inverted pendulum model that are stable only in a restricted range of *Froude numbers*, while they become unstable for smaller or larger *Froude numbers*.

1. Introduction

Locomotion shapes form and function through the environment (Alexander, 1981, 1989, 2003a; Patek and Biewener, 2018) and performing movements efficiently is key for survival of terrestrial and other species (Foster et al., 2015; Dickinson et al., 2000; Garland and Losos, 1994). The large diversity of morphologies and locomotor gaits interests researchers who try to understand how animals move through their habitat and why different species hop, run, or walk or why they move bipedally, quadrupedally, or multipedally (Alexander, 2003a; Gordon et al., 2017) on horizontal (Geyer et al., 2005; Seyfarth et al., 2002) and other surfaces, such as declines (Birn-Jeffery and Higham, 2014), inclines (Birn-Jeffery and Higham, 2014; Selvitella and Foster, 2022b; Foster and Selvitella, 2022b,a; Selvitella and Foster, 2022a), steps (Birn-Jeffery et al., 2014), and uneven ground (Müller et al., 2016). The complexity of locomotion is such that the performance of natural species is still superior to those of robots and engineers have not yet been able to replicate the efficiency of animal locomotion in artificial creatures (Raibert, 1986; Raibert et al., 2008). Although some progress has been made (Full and Koditschek, 1999; Ghigliazza and Holmes, 2005; Geyer et al., 2006b), it is very complicated to fully describe, through a mathematical model, the interaction and cooperation between the nervous and the musculoskeletal systems, whose fundamental principles are still largely unknown (Holmes et al., 2006; Gordon et al., 2017; Alexander, 2003b). Conceptual (Margaria, 1976; Cavagna et al., 1977; Coleman et al., 1997), physical (McGeer, 1990b,a; Iida et al., 2008; Seok et al., 2013), and mathematical (Blickhan, 1989; McMahon and Cheng, 1990; Ghigliazza et al., 2003) descriptions have been employed to shed light on the nature and the diversity of locomotor behavior of humans and of other animals.

* Corresponding author at: Department of Mathematical Sciences, Purdue University Fort Wayne, 2101 E Coliseum Blvd, Fort Wayne, IN, 46805, United States of America.
E-mail addresses: aselvite@pfw.edu (A.M. Selvitella), klfoster@bsu.edu (K.L. Foster).

https://doi.org/10.1016/j.jtbi.2024.111934
Received 21 January 2024; Received in revised form 24 August 2024; Accepted 29 August 2024
Available online 4 September 2024

Reductionist models are mathematical models that take the form of dynamical systems and aim to describe a gait through the least possible number of variables (Usherwood, 2010, 2016, 2020; Croft et al., 2017). Such models have been able to explain the main features of terrestrial legged locomotion (Blickhan and Full, 1993; Holmes et al., 2006; Geyer et al., 2006a; Alexander, 2003b) using interpretable low dimensional systems of nonlinear differential equations, mainly concentrating on the dynamics of the center of mass (CoM) (Dickinson et al., 2000; Alexander, 2003b; Geyer, 2005). Among the most successful systems are the inverted pendulum and spring–mass models such as the spring loaded inverted pendulum (SLIP). The SLIP model has been successful in describing the compliant dynamics of hopping (Farley et al., 1991; Seyfarth et al., 2001; Gordon et al., 2017) in one dimension (vertical) and of running in two dimensions (sagittal plane) (Blickhan, 1989; McMahon and Cheng, 1990; Gordon et al., 2017; Farley et al., 1993). Historically, walking was modeled using an inverted pendulum (Cavagna and Margaria, 1966; Cavagna et al., 1963, 1977; Alexander, 1976; Mochon and McMahon, 1980; Srinivasan and Ruina, 2005) (see also (Gordon et al., 2017) for an extended list of references), while, more recently, an extension of the SLIP model that includes the possibility of double support during stance has been able to reproduce more accurately the ground reaction forces acting on the CoM during the contact phase (Geyer et al., 2006a). Several robots capable of running successfully are controlled using SLIP-based models (Raibert, 1986; Saranli and Koditschek, 2003; Westervelt et al., 2003; Poulakakis and Grizzle, 2009). In Full and Koditschek (1999), authors suggest that the SLIP models the most essential features of sagittal plane dynamics of the CoM of many animal species, including cockroaches, dogs, kangaroos, birds, and humans. Furthermore, Blickhan and Full (1993) showed that the SLIP model can accurately predict the energetics and dynamics of trotting, running, and hopping in a multitude of animal species (see also Dickinson et al., 2000).

Even if conceptually simple, the SLIP model can describe a rich dynamics (Gordon et al., 2017; Patek and Biewener, 2018; Holmes et al., 2006). The SLIP dynamical system that describes running is *hybrid* (Goebel et al., 2012; van der Schaft and Schumacher, 2000) in the sense that it involves two phases, a stance phase and a flight phase for each stride, and a combination of continuous and discrete components. The SLIP model is also *piecewise holonomic* (Geyer et al., 2005; Ruina, 1998; Holmes et al., 2006) in the sense that it is smooth and holonomic everywhere except at the instants of transition (Ruina, 1998; Holmes et al., 2006; Geyer et al., 2005; Coleman et al., 1997; Coleman and Holmes, 1999). Two different vector fields describe the two phases and they switch at the times of touch-down and take-off. During stance, a leg is in contact with the ground and the CoM is subject to the gravitational force $F_g = mg$ ($g = 9.81\ \mathrm{m/s^2}$ is the gravitational constant, m the mass of the individual concentrated in the CoM), but also to the ground reaction forces (which are transmitted directly to the CoM from the foot) and the elastic force with constant linear stiffness $k < +\infty$ of the massless leg spring of length l_0. During stance, the compliant, massless leg rotates around the foot. The stance phase begins and ends with a straight leg (no leg compression) following the flight phase. During the flight phase, the motion is ballistic and only the gravitational force acts on the CoM, until the foot hits the ground with an angle of attack α_0, which is constant in each stride. The dynamics is constrained by other conditions: the apex height, which is reached during flight, must be higher than the touch-down height, and the leg cannot crash into the ground. See Fig. 1 and Table 1 for more details on the parameters of the model.

Hybrid systems describing the dynamics of the CoM during terrestrial locomotion admit asymptotically stable periodic trajectories (Seyfarth et al., 2002; Ghigliazza et al., 2003; Ruina, 1998; Coleman et al., 1997; Coleman and Holmes, 1999). The difficulty in proving the existence of periodic motions for these models and in investigating their stability properties is a reflection of the lack of regularity of the transition maps between stance and flight phases and, in fact, a consequence of the hybrid nature of the dynamical systems. Note that dynamical systems that are holonomic and conservative do not possess solutions which are asymptotically stable (Holmes et al., 2006). The fact that these SLIP conservative systems are only piecewise holonomic is the key for the (partial) asymptotic stability of periodic orbits (Seipel and Holmes, 2005; Ruina, 1998). Most often, the existence of periodic orbits for hybrid systems is proven by showing the existence of fixed points of Poincaré maps, such as the apex return map, while the stability of such periodic orbits is proven through the study of the contractive properties of these Poincaré maps. Especially in the robotics literature and control theory, this attractive feature of periodic orbits is called *self-stability* (Seyfarth et al., 2002; Geyer et al., 2005; Ghigliazza et al., 2003; Geyer, 2005) because this type of stability is intrinsic to the model and does not need any continuous sensory feedback.

Hybrid models of legged locomotion very rarely admit exact solutions that can be expressed in simple forms, other than under regimes which might lack biological significance, such as those assuming a negligible effect of gravity during stance ($g = 0$) (Ghigliazza et al., 2003). Perturbative approaches which take the effect of gravity during stance into consideration have been used too (Schwind, 1998; Schwind and Koditschek, 2000; Geyer, 2001; Yu et al., 2012), but often they lack a simple interpretation of how the parameters of the model affect important biomechanical variables, such as the maximal leg compression or the angle swept during stance. Another approach uses approximations of the dynamics under biologically meaningful assumptions, such as small compression or small angle swept during stance (Geyer et al., 2005; Yu et al., 2012; Shahbazi et al., 2016; Kilic and Braun, 2023). The resulting approximate models can be often solved in terms of elementary functions (Geyer et al., 2005; Selvitella and Foster, 2022b,a) and have been useful for the derivation of formulas for parameters of biomechanical interest and the study of gait stability. The authors in Geyer et al. (2005) produce a solution of the SLIP model that includes gravity and that is exact during the flight phase, while it is approximate during the stance phase. During stance, the solution in Geyer et al. (2005) is oscillatory in the radial variable and linear plus oscillatory in the angular variable. With this approximation, the authors were able to calculate explicit approximate formulas for the duration of the stance phase and for the angle swept during stance. The angle swept during stance is very important for stability purposes because it appears in the calculation of the apex return map and so it impacts both the existence of periodic gaits and their asymptotic stability. Even in the approximation used in Geyer et al. (2005), the form of the apex return map, especially in the component that depends on the stance dynamics (e.g. the angle swept during stance), is so complicated that the authors prove existence of periodic solutions only under the condition that the stance phase dynamics is symmetric around midstance and under the restrictive condition that the angular velocity at touch-down is identical to the pendulum frequency $\omega = -\sqrt{g/l_0}$ (forward motion).

In this paper, we push the reduction of the dynamics one step further by using an approximation for the angular variable at a lower order than the one used in Geyer et al. (2005) and we discuss the full stability problem without the restriction on the angular velocity used in Geyer et al. (2005). In more precise terms, we approximate the angular dynamics to only linear in time, which corresponds to the approximation of the angular variable in Geyer et al. (2005) at 0-th order, instead of 1-st order. The radial component of our approximation is very similar to that in Geyer et al. (2005), with the only difference that the potential energy is approximated with a potential energy that matches the correct potential energy at touch-down (and at take-off, given that we consider only symmetric stance phases too) instead of at midstance used in Geyer et al. (2005). This allows the approximate system to have the same energy of the original system when the other parameters of both the approximate and exact models are kept with the same values (See Remark 2.1 below). Given that in both (Geyer et al., 2005) and here, we restrict the dynamics to the case of small angle swept during stance, the difference is negligible in terms of accuracy of the approximation of the dynamics of the radial variable (See Section 2.2 and Appendix A.4). Similar assumptions are present in Yu et al. (2012) (formula (4), page 4198) and in other references,

Table 1
This table defines the main parameters and variables of our model.

Parameters and variables	
Parameter/variable	Definition
l_0	Resting length of the leg
α_0	Angle of attack of the leg relative to the ground
m	Point mass
$g = 9.81$ m/s	Gravitational constant
k	Stiffness of the spring/leg
ω_0	Linear spring frequency
ω	Angular velocity of the CoM during stance
t	Time
t_{TD}	Time of touch-down
t_{TO}	Time of take-off
ϕ	Angular position of the CoM during stance
$\Delta\phi$	Angle swept by the CoM during stance
r	Radial position of the CoM during stance
P	Angular momentum during stance
E	System energy
a	Relative height of oscillation of the CoM during stance
b	Relative amplitude of oscillation of the CoM during stance
ρ	Relative spring amplitude of the CoM during stance
$\tilde{k}$	Dimensionless stiffness of the spring/leg
$\tilde{E}$	Dimensionless system energy
ϵ	Relative system energy
Fr	Froude number

including (Arslan et al., 2009; Saranlı et al., 2010; Schwind, 1998; Uyanık et al., 2015; Yu et al., 2021). Without imposing that the angular velocity at touch-down must be identical to the pendulum frequency, the apex return map, and so its fixed points and their stability, show an explicit dependence on a fundamental biomechanical quantity, a version of the *Froude number* ($Fr := \omega^2 l_0/g$), which regulates the exchange between potential and kinetic energy and the transitions between gaits (Alexander, 2003a). The appearance of an explicit dependence of the apex return map on Fr is relatively new in the sense that imposing $\omega = -\sqrt{g/l_0}$ was implicitly implying $Fr = 1$ (as already noted in Geyer et al., 2005) and was reducing the richness of the parameter space by one dimension. In our case, the existence and stability of fixed points of the apex return map depend not only on the normalized stiffness $\tilde{k}$ (see Section 2.1 below), the normalized energy $\tilde{E}$ (see Section 2.1 below), and the angle of attack α_0, but also on the *Froude number* Fr. This extra flexibility is crucial in the proof of a bifurcation phenomenon that we highlight in this paper: we give examples of stable running gaits becoming unstable when Fr is moved outside an explicit interval. We validate our hypotheses and our analysis using a dataset of humans running on a treadmill at different velocities, publicly available from Fukuchi et al. (2017). We show that the hypothesis of constant angular velocity is valid.

In summary, (1) we propose an approximation of the SLIP model with constant angular velocity during stance; (2) we show that with the additional assumptions of little to no leg compression and symmetric stance phase, which are commonly used in the literature, we can compute the apex return map with elementary functions; (3) we demonstrate that, under this regime, we can derive stability conditions in terms of elementary functions; (4) we show that the *Froude number* appears as a parameter which induces a bifurcation that destabilizes the running gait outside a certain range; and (5) using publicly available data of human running on a treadmill, we validate our modeling assumptions, in particular the assumption that the angular velocity of the body around the toe during stance can be well approximated as linear in time. These contributions connect with many research endeavours in the biomechanics literature.

Some of our analysis relates to a question posed in Holmes et al. (2006) (page 263). There, authors discuss the difficulty in interpreting Taylor series approximations of periodic solutions of the SLIP model and how researchers use approximations around midstance, small compressions, and leg angles close to vertical to derive explicit solutions valid under these regimes. The authors in Holmes et al. (2006) ask for which species particular approximations are most suitable and if more elegant approximations may be found. Our analysis answers some parts of this question because we show that the simplified approximation of constant angular velocity during stance is well suited for some data of humans running on a treadmill. The assumptions of small compression and small length during stance are ubiquitous in the literature (see for example Geyer et al., 2005; Holmes et al., 2006 and references therein). We include the effect of gravity during stance in contrast to earlier studies (Geyer, 2001; Ghigliazza et al., 2003). The authors in Ghigliazza et al. (2003) derive explicit Poincaré maps to obtain simple expressions for periodic solutions and their stability, and to illustrate bifurcation phenomena. The deductions in Ghigliazza et al. (2003) concentrate on the integrable case, namely that in which gravity is neglected (or high stiffness) during stance and the authors provide numerical evidence that their work is relevant also when gravity is reintroduced. Note that their result in fact considers a restricted regime, or at least a very different regime, with respect to ours because, if $g \to 0$ and all other parameters are kept fixed, then $Fr \to +\infty$, while our analysis is valid also for $Fr < +\infty$. Ghigliazza et al. (2003) do not compare the validity of their model with specific animal species and complement the experimental study of Seyfarth et al. (2002), in which the authors found self-stabilizing behaviors for fast enough running, suitable leg stiffness, and for a range of fixed angles of attack, via numerical simulations.

Authors in Yu et al. (2012) obtain highly accurate analytic approximate solutions to the SLIP dynamics in stance phase with gravity under the assumptions of small angular span and relative small compression, in particular for non-symmetric dynamics in a large angle range. Differently from our approach, they do not assume symmetric stance phase in their approximation, but they use a higher order angular dynamics, and so a more complex angular dynamics than the one with constant angular velocity. The approximation in Kilic and Braun (2023) to the SLIP model does not rely on the assumptions of symmetric stance phase and replaces the assumption of small step length with that of small vertical displacement, which are relevant cases in the study of the fast walking of robots. To reach high accuracy, the authors increase the complexity of the model of the spring force by introducing a sine wave approximation of the horizontal ground reaction force. Furthermore, Shahbazi et al. (2016) presents a unified framework for active running, walking, and walk–run transitions, by introducing an axial-torsional SLIP (AT-SLIP) for the double-stance phase, which is absent during running. Authors find that AT-SLIP trajectories approximate accurately the bipedal SLIP during the double stance

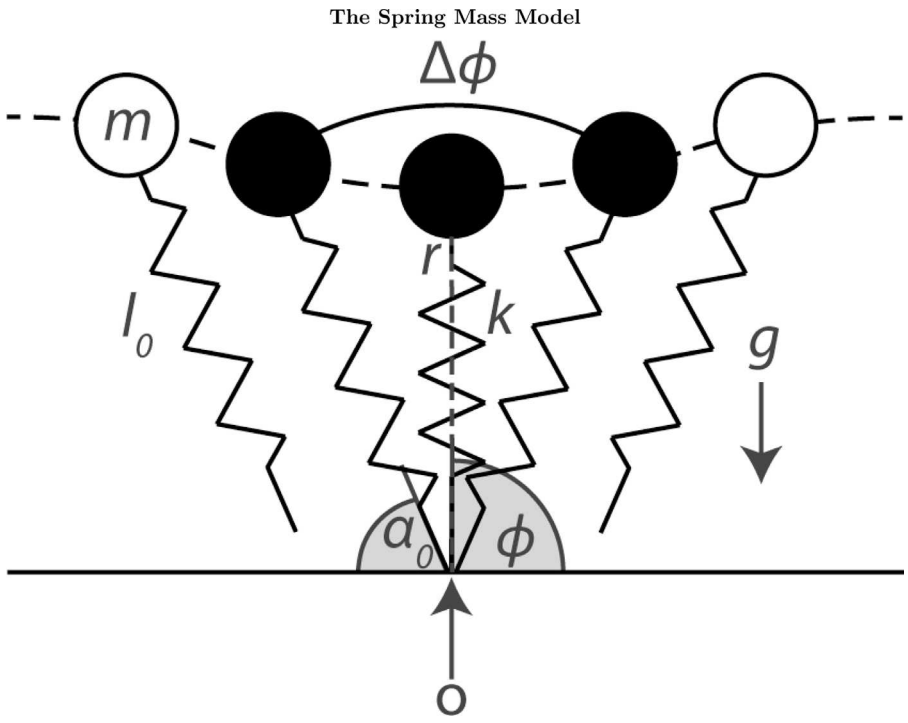

Fig. 1. The spring–mass model. This picture illustrates the stance dynamics of the SLIP model. The parameters considered are: the gravitational constant $g = 9.81$ m/s^2; α_0 with $\pi - \alpha_0$ representing the angle of attack, k representing the leg stiffness of the massless leg; m representing the mass of the individual concentrated in the CoM; and the leg length l_0. O is the contact point. The variables considered in the model are: the angle ϕ measured counterclockwise with $\Delta\phi < 0$ being the angle swept during stance and the distance r of the CoM from the point of contact with the ground.

phase, under the assumption of small angle swept during stance and small leg compression. This work expands on Geyer et al. (2005) and Arslan et al. (2009) and is particularly relevant when the stance dynamics is not symmetric. The papers (Yu et al., 2012; Kilic and Braun, 2023; Shahbazi et al., 2016) simulate their models with parameters emerging from biological data relevant to human locomotion, but do not directly fit their models to experimental data.

The paper is organized as follows. In Section 2, we discussed the methodology developed in this paper. In particular: Section 2.1 describes our approximation and the formula for the angle swept during stance; Section 2.2 describes the apex return map and it is dedicated to the stability analysis. There, we derive the apex return map, an explicit formula for the apex height for constant angular velocity during stance, and the conditions for stability of periodic gaits. Section 3 is devoted to the results: Section 3.1 describes the data considered in our analysis; Section 3.2 verifies the validity of our hypothesis of constant angular velocity and the accuracy of the approximate radial and angular dynamics; and Section 3.3 proves the existence of parameters of our model that allow a symmetric stance phase. In Section 4, we discuss our results: In particular, the pros and cons of our approximation (Section 4.1), the bifurcation phenomenon (Section 4.2), the issue of asymmetric gaits (Section 4.3), and some further considerations in Section 4.4. In Section 5, we draw our conclusions. In the Appendix (Appendix), we include the mathematical deductions which led to the model and the formulas used in this paper. In particular: Appendix A.1 reports the calculation of the angle swept during stance; Appendix A.2 gives details about the derivation of the formula for the apex return map; Appendix A.3 reports the calculation of the fixed point of the apex return map; and Appendix A.4 reports the proof of the stability condition of fixed points of the apex return map under the assumptions of our approximation. In Appendix A.5, we perform an error analysis for the apex return map with our approximation. In Appendix A.6, we report further results of our data analysis, while in Appendix A.7 we provide a point-by-point comparison of our approximation with that of Geyer et al. (2005).

2. Theory

This section is dedicated to the methodology developed in this paper, including our approximation of the SLIP model (Section 2.1) and a description of the apex return map and the explicit expression of the stability conditions for symmetric periodic gaits under the regime of linear angular dynamics (Section 2.2).

2.1. The approximate solution

In the SLIP model, the aerial phase of the motion is described with a ballistic motion. On the other hand, each stance phase is governed by the Lagrangian:

$$L = \frac{m}{2}\left(\dot{r}^2 + r^2\dot{\phi}^2\right) - \frac{k}{2}\left(l_0 - r\right)^2 - mgr\sin(\phi). \tag{1}$$

Here, $r \in [0, l_0)$ represents the radial coordinate of the point mass with respect to the contact point and $\dot{r}$ its variation, while $\phi \in [0, \pi)$ represents the angle oriented from the ground (flat surface) to the leg (counterclockwise) and $\dot{\phi}$ its derivative (See Fig. 1 or Figure 1 in Geyer et al. (2005)).

The Lagrange equations of this model are not integrable in the sense that they do not admit solutions in terms of elementary functions (Whittacker, 1904; Holmes et al., 2006; Geyer et al., 2005), unless in trivial cases, and so solutions are often found numerically (Holmes et al., 2006; Schwind and Koditschek, 2000) or through approximate methods (Geyer et al., 2005). In Geyer et al. (2005), the authors concentrated on the SLIP dynamics for small angle swept during stance $\phi \sim \frac{\pi}{2}$ and small leg compression $\rho := (r - l_0)/l_0 \ll 1$. Under this regime, the authors were able to provide explicit solutions for the radial and angular variables, together with an explicit formula for the angle swept during stance $\Delta\phi$. Moreover, under the restriction that the system is oscillating with the pendulum frequency $\omega = -\sqrt{\frac{g}{l_0}}$, Geyer et al. (2005) derived a condition for the stability of periodic solutions with a symmetric stance phase ($\Delta\phi = 2\alpha_0 - \pi$).

Here, we approximate the stance dynamics of the SLIP model even further with respect to what is done in Geyer et al. (2005). In particular, we approximate the angular dynamics

$$\dot{\phi} = \frac{\omega}{(1+\rho)^2}$$

at zero order, namely one order less that the approximation performed by Geyer et al. (2005), which approximated the angular dynamics with $\dot{\phi} \simeq \omega(1 - 2\rho)$. Therefore, we consider constant angular velocity during stance:

$$\dot{\phi} = \omega < 0.$$

The negative sign comes from the fact that we are only interested in forward motion. Imposing this condition and that of $\phi \sim \alpha_0$, we obtain a reduced Lagrangian

$$L = \frac{m}{2}\left(\dot{r}^2 + r^2\omega^2\right) - \frac{k}{2}\left(l_0 - r\right)^2 - mgr\sin(\alpha_0)$$

with energy given by:

$$E = \frac{m}{2}\left(\dot{r}^2 + r^2\omega^2\right) + \frac{k}{2}\left(l_0 - r\right)^2 + mgr\sin(\alpha_0).$$

Here $0 < \alpha_0 < \frac{\pi}{2}$. Note that the potential energy E_{pot} is approximated slightly differently with respect to that in Geyer et al. (2005), where it is approximated by mgr. Instead, we approximate E_{pot} with potential energy that matches the correct potential energy at touch-down, $mgr\sin\alpha_0$. Given that $\phi \sim \alpha_0 \sim \frac{\pi}{2}$, the difference between the two approximations is small. Similar to Geyer et al. (2005), we re-scale the equations of motion, but differently from Geyer et al. (2005), by normalizing with respect to ω^2, instead of normalizing with respect to g/l_0. Our normalization is equivalent to that in Geyer et al. (2005), in the case of $Fr = 1$ considered in Geyer et al. (2005). If we define $\tilde{k} := \frac{k}{m\omega^2}$, $\tilde{E} := \frac{E}{ml_0^2\omega^2}$, and $\epsilon := \frac{2E}{ml_0^2}$, we get

$$\epsilon = \dot{\rho}^2 + \frac{\omega^2}{(1+\rho)^2} + \omega_0^2\rho^2 + \frac{2(g\sin\alpha_0)}{l_0}(1+\rho),$$

with $\omega_0 = \sqrt{k/m}$ representing the linear spring frequency. Approximating for small compression $\rho := (r - l_0)/l_0 \leq 0$ and $|\rho| \ll 1$ and using McLaurin expansion $(1+\rho)^{-2} = 1 - 2 * \rho + 3 * \rho^2 + O(\rho^3)$, we obtain

$$\epsilon = \dot{\rho}^2 + \omega^2(1 - 2\rho + 3\rho^2) + \omega_0^2\rho^2 + \frac{2(g\sin\alpha_0)}{l_0}(1+\rho).$$

This equation can be solved by separation of variables. We keep $\dot{\rho}^2$ on one side of the equality and move everything else on the other side. We obtain:

$$\epsilon - \omega^2(1 - 2\rho + 3\rho^2) - \omega_0^2\rho^2 - \frac{2(g\sin\alpha_0)}{l_0}(1+\rho) = \dot{\rho}^2.$$

If we take the square root on both sides and separate variables (dt on the left and everything else on the right of the equal sign), we get

$$dt = \frac{d\rho}{\sqrt{\epsilon - \omega^2(1 - 2\rho + 3\rho^2) - \omega_0^2\rho^2 - \frac{2(g\sin\alpha_0)}{l_0}(1+\rho)}}.$$

Integrating from time 0 to t, we get

$$t = \int \frac{d\rho}{\sqrt{\lambda\rho^2 + \mu\rho + \nu}} = -\frac{1}{\sqrt{-\lambda}}\arcsin\frac{2\lambda\rho + \mu}{\sqrt{\mu^2 - 4\lambda\nu}}$$

with $\lambda = -(3\omega^2 + \omega_0^2)$, $\mu = 2(\omega^2 - (g\sin\alpha_0)/l_0)$, and $\nu = \epsilon - \omega^2 - 2(g\sin\alpha_0)/l_0$. Note that $\nu = \dot{r}_0^2/l_0^2 > 0$ (see Remark 2.1 below). Solving this and getting back to the original variables, we arrive at the formula for the radial motion, given by:

$$r(t) = l_0\left(1 + a + b\sin\hat{\omega}_0 t\right) \tag{2}$$

with

$$a = \frac{\omega^2 - (g\sin\alpha_0)/l_0}{\omega_0^2 + 3\omega^2}$$

and

$$b = \frac{\sqrt{(\omega^2 - (g\sin\alpha_0)/l)^2 + (\omega_0^2 + 3\omega^2)(\epsilon - \omega^2 - 2(g\sin\alpha_0)/l_0)}}{\omega_0^2 + \omega^2}.$$

Here $\hat{\omega}_0 := \sqrt{\omega_0^2 + 3\omega^2}$. The radial solution is very similar to that in Geyer et al. (2005), but with a factor of $\sin\alpha_0$ appearing as a multiplier of g. By imposing the touch-down and take-off conditions $r(t_{TD}) = r(t_{TO}) = l_0$, we obtain the times of touch-down and take-off, respectively:

$$t_{TD} = \frac{1}{\hat{\omega}_0}\left\{\left(2n + \frac{3}{2}\right)\pi - \left[\frac{\pi}{2} + \arcsin\left(-\frac{a}{b}\right)\right]\right\}$$

and

$$t_{TO} = \frac{1}{\hat{\omega}_0}\left\{\left(2n+\frac{3}{2}\right)\pi + \left[\frac{\pi}{2} + \arcsin\left(-\frac{a}{b}\right)\right]\right\},$$

with $n \in \mathbb{Z}$. From this, we can compute the angle swept during stance

$$\Delta\phi = \int_{t_{TD}}^{t_{TO}} \dot{\phi} dt = \int_{t_{TD}}^{t_{TO}} \omega dt = \omega(t_{TO} - t_{TD}) = \frac{\omega}{\hat{\omega}_0}\left\{\pi + 2\arcsin\left(-\frac{a}{b}\right)\right\},$$

which implies

$$\Delta\phi = 2\frac{\omega}{\hat{\omega}_0}\left\{\arccos\left(\frac{a}{b}\right)\right\}$$

and so, dividing numerator and denominator by ω^2, we obtain

$$\Delta\phi(\tilde{k}, \alpha_0, \tilde{E}) = -\frac{2}{\sqrt{\tilde{k}+3}} \arccos\left\{\frac{1 - \sin\alpha_0/Fr}{\sqrt{(1-\sin\alpha_0/Fr)^2 + (\tilde{k}+3)(2\tilde{E} - 1 - 2\sin\alpha_0/Fr)}}\right\} \tag{3}$$

with

$$Fr := \frac{\omega^2 l_0}{g}$$

playing the role of the *Froude number*. For the full list of parameters and variables, please see Table 1.

Remark 2.1. As mentioned above, authors in Geyer et al. (2005) approximated the potential energy during stance E_{pot} with a potential energy that matches the correct potential energy at mid-stance, $E_{pot} \sim mgr$, while we approximate E_{pot} with a potential energy that matches the correct potential energy at touch-down, $E_{pot} \sim mgr\sin\alpha_0$. The difference in accuracy is small because $\phi \sim \alpha_0 \sim \frac{\pi}{2}$. Other approximations can be done. With minimal adjustments, all the computations in this paper are valid if the potential energy is approximated with $mgr\sin(\beta)$ with $\alpha_0 \leq \beta \leq \pi/2$, which includes the strategy implemented in Geyer et al. (2005) ($\beta = \pi/2$). For example, we would still have $\nu = \dot{r}_0^2/l_0^2 > 0$, but with the proper definition $\nu = \epsilon - \omega^2 - 2(g\sin\beta)/l_0$, and we would still have $2\tilde{E} - 1 - 2\sin\alpha_0/Fr \geq 0$ (See Section 2.2 and the formula for the stability condition available in Eq. (9)). However, our choice ($\beta = \alpha_0$) is the only case for which the energy at touch down is identical for both the approximate and the exact SLIP dynamics. Given the conservative nature of both the true and the approximate stance dynamics (with respect to the respective flows), the energy during stance for both the approximate and exact models are identical, using our approximation. This is important for the purpose of inferring properties of the true dynamics from those of the approximate dynamics. An example of this is the bifurcation phenomenon described in Section 4.2, where it is highlighted that the stability of a fixed point of the apex return map depends on the energy.

2.2. The apex return map and the stability of periodic gaits

To study the stability properties of the periodic solutions to the SLIP model, we study the fixed points of the apex return map. The apex return map is a Poincaré map, namely a discrete dynamical system deduced from the original dynamics by intersecting a periodic orbit in the state space with an hyperplane or a submanifold of the state space, called the Poincaré section, transverse to the flow. It is convenient to consider the apex height as the coordinate of the section because it allows for an explicit, relatively simple representation of the map as a discrete one-dimensional system, whose only variable is the apex height y_i during stance i. If the eigenvalues of the linearization of the apex return map around a fixed point are within the unit circle for a certain range of the parameters, then the fixed-point is stable for that range of parameters. Note that a periodic gait can be stable for a certain set of parameters and unstable for another.

2.2.1. The apex return map

The apex-return map is a discrete map f, which recursively determines the highest vertical position y_{i+i} in stride $i+1$ from the highest vertical position y_i in stride i. A way to determine f is by composition of five maps $f = f_- \circ T \circ f_0 \circ T^{-1} \circ f_+$, with f_- being the apex i to touch down $i+1$ map (flight phase); f_0 being the touch down $i+1$ to take off $i+1$ map (stance phase); f_+ being the take off $i+1$ to apex $i+1$ map, and T and T^{-1} being the change of variables map from Euclidean to polar coordinates and its inverse (well defined as $r > 0$ during stance). During the flight phase, most suitable coordinates are the Euclidean ones, while during the stance phase polar coordinates simplify the description of the dynamics. Therefore, change of variables at touch down and take off need to be used. In their respective coordinate frames, we have that the y_i to touch down map is given by

$$f_- = \begin{cases} \dot{x}_i = \dot{x}_{TD} = \sqrt{\frac{2}{m}(E - mgy_i)} \\ y_{TD} = l_0\sin\alpha_0 \\ \dot{y}_{TD} = -\sqrt{2g(y_i - y_{TD})}, \end{cases} \tag{4}$$

the touch down to take off map is given by

$$f_0 = \begin{cases} r_{TO} = r_{TD} \\ \dot{r}_{TO} = -\dot{r}_{TD} \\ \phi_{TO} = \phi_{TD} + \Delta\phi \\ \dot{\phi}_{TO} = \dot{\phi}_{TD}, \end{cases} \tag{5}$$

and the take off to y_{i+1} map is given by

$$f_+ = \begin{cases} \dot{x}_{i+1} = \dot{x}_{TO} \\ y_{i+1} = y_{TO} + \frac{1}{2g}\dot{y}_{TO}^2. \end{cases} \tag{6}$$

Remark 2.2. A similar formula was derived in Geyer et al. (2005). However, their expression (25) on page 345 is incorrect (there is a square missing in their formula for y_{i+1}, where $\dot{y}_{TO}$ appears only as a linear term). This is probably just a typo, as formula (26) on page 345 in Geyer et al. (2005) is actually correct.

The apex return map for the SLIP model is then given by:

$$y_{i+1} = f(y_i) = \frac{1}{mg}\left[\cos(\Delta\phi - 2\alpha_0)\sqrt{mg(y_i - l_0\sin\alpha_0)} + \sin(\Delta\phi - 2\alpha_0)\sqrt{E - mgy_i}\right]^2 + l_0\sin(\alpha_0 - \Delta\phi) \tag{7}$$

under the condition that the apex height is higher than the touch-down height

$$y_{i+1} \geq l_0\sin(\alpha_0),$$

which ensures that the apex return map exists. The full derivation of this formula is given in Appendix A.2.

Remark 2.3. We report the computation of the full derivation of the apex return map in Appendix A.2 to avoid confusion with respect to the apex return map formula in Geyer et al. (2005), page 345. The authors in Geyer et al. (2005), in their derivation of the apex return map described on page 345, do not explicitly say that their formula (26) is valid also for the exact, non-approximated dynamics. The approximation enters crucially later on in that section, when actual computations using the approximation formula for $\Delta\phi$ are reported. Formula (26) in Geyer et al. (2005) and our formula (7) depend on the stance dynamics only through $\Delta\phi$. Therefore, the apex return map, **as a function of** $\Delta\phi$, is identical independently of what explicit formula would be then substituted in $\Delta\phi$. The approximation helps computing this $\Delta\phi$ as a function of the other parameters but not to compute the apex return map as a function of $\Delta\phi$ in both our work and Geyer et al. (2005). However, our work is largely distinct from Geyer et al. (2005) in the way $\Delta\phi$ is computed, as we use a simpler approximation (e.g. linear angular dynamics during stance) with respect to the one used in Geyer et al. (2005) and we do not restrict the analysis to the case $Fr = 1$. These two differences led to (1) showing that, for human subjects running on a treadmill, the CoM is well described by a linear angular dynamics (see Section 3.2 below) and (2) the appearance of a bifurcation phenomenon with Fr as a bifurcation parameter (see Section 4.3 below).

By rescaling $Y_i := y_i/l_0$ and $F(Y_i) := f(y_i)/l_0$, we get

$$Y_{i+1} = F(Y_i) = \left[\cos(\Delta\phi - 2\alpha_0)\sqrt{Y_i - \sin\alpha_0} + \sin(\Delta\phi - 2\alpha_0)\sqrt{\tilde{E}Fr - Y_i}\right]^2 + \sin(\alpha_0 - \Delta\phi). \tag{8}$$

Note that $\tilde{E}Fr = E/(mgl_0)$ is independent of ω^2. For Eq. (8) to be valid, we need to have the restriction

$$\tilde{E}Fr \geq Y_i \geq \sin\alpha_0.$$

Note that

$$2\tilde{E} - 1 - 2\sin\alpha_0/Fr \geq 0,$$

since

$$\omega^2(\tilde{E} - 1 - 2\sin\alpha_0/Fr) = \epsilon - \omega^2 - 2(g\sin\alpha_0)/l_0 = \nu = \dot{r}_0^2/l_0^2 > 0.$$

Manipulating the expression $\tilde{E}Fr \geq Y_i \geq \sin\alpha_0$, we get

$$\tilde{E}Fr \geq \frac{Fr}{2} + \sin\alpha_0 \geq \sin\alpha_0$$

and so the condition $\tilde{E}Fr \geq Y_i \geq \sin\alpha_0$ is not void.

Remark 2.4. In Appendix A.5, we show that the error in the apex return map that we make is small for small compression.

2.2.2. Explicit formula of the apex height

The solution to the approximate SLIP dynamics admits an explicit representation of the apex height for each stance i as a function of the parameters of the model. Using the formula for the angular velocity at touch-down in polar coordinates (equation (24) in Geyer et al. (2005)), we get:

$$\omega = \sqrt{\frac{2g}{l_0}}\left(\cos\alpha_0\sqrt{Y_i - \sin\alpha_0} - \sin\alpha_0\sqrt{\tilde{E}Fr - Y_i}\right),$$

which, since we are considering only forward motion and so $\omega < 0$, reduces to

$$-\sqrt{\frac{Fr}{2}} = \cos\alpha_0\sqrt{Y_i - \sin\alpha_0} - \sin\alpha_0\sqrt{\tilde{E}Fr - Y_i}.$$

After some manipulations (see Appendix A.3), we can solve for Y_i and obtain

$$Y_i = \sin\alpha_0 + \frac{1}{2}\left(\sqrt{Fr}\cos\alpha_0 \pm \sin\alpha_0\sqrt{\{-Fr + 2\tilde{E}Fr - 2\sin\alpha_0\}}\right)^2.$$

With similar computations, we get

$$Y_i = \tilde{E}Fr - \frac{1}{2}\left(\sqrt{Fr}\sin\alpha_0 \pm \cos\alpha_0\sqrt{\{-Fr + 2\tilde{E}Fr - 2\sin\alpha_0\}}\right)^2.$$

By plugging these solutions into the condition

$$-\sqrt{\frac{Fr}{2}} = \cos\alpha_0\sqrt{Y_i - \sin\alpha_0} - \sin\alpha_0\sqrt{\tilde{E}Fr - Y_i},$$

we get that the only possible solutions are

$$Y_i = \sin\alpha_0 + \frac{1}{2}\left(\sqrt{Fr}\cos\alpha_0 - \sin\alpha_0\sqrt{\{-Fr + 2\tilde{E}Fr - 2\sin\alpha_0\}}\right)^2$$

$$= \tilde{E}Fr - \frac{1}{2}\left(\sqrt{Fr}\sin\alpha_0 + \cos\alpha_0\sqrt{\{-Fr + 2\tilde{E}Fr - 2\sin\alpha_0\}}\right)^2.$$

See Appendix A.3 for more details about this computation. As a by-product, this formula gives us the formula for the minimal energy E^{min} needed for a fixed point of the apex return map F to exist. In fact, since we need to satisfy $Y_i > \sin\alpha_0$, E^{min} must satisfy

$$\frac{1}{2}\left(\sqrt{Fr}\cos\alpha_0 - \sin\alpha_0\sqrt{\{-Fr + 2\tilde{E}Fr - 2\sin\alpha_0\}}\right)^2 = 0$$

and so

$$\tilde{E}^{min} = \frac{1}{2\sin^2\alpha_0} + \frac{\sin\alpha_0}{Fr}.$$

This generalizes to every $Fr > 0$, the energy lower bound found in Geyer et al. (2005) for $Fr = 1$.

2.2.3. Asymptotic stability of periodic gaits

Expanding $F(Y_i)$ from Eq. (8), we get

$$F(Y_i) = \cos^2(\Delta\phi - 2\alpha_0)\left[Y_i - \sin\alpha_0\right] + \sin^2(\Delta\phi - 2\alpha_0)\left[\tilde{E}Fr - Y_i\right] + \sin(2[\Delta\phi - 2\alpha_0])\sqrt{Y_i - \sin\alpha_0}\sqrt{\tilde{E}Fr - Y_i} + \sin(\alpha_0 - \Delta\phi).$$

For the stability of the apex return map, we need

$$\left|\frac{\partial F}{\partial Y_i}\right|_{Y_{i+1}=Y_i} < 1.$$

Given that at the symmetric fixed point $Y_{i+1} = Y_i$, we have $\Delta\phi = 2\alpha_0 - \pi$, we obtain

$$\frac{\partial F}{\partial Y_i}\Big|_{Y_{i+1}=Y_i} = \frac{\partial F}{\partial Y_i}\Big|_{\Delta\phi=2\alpha_0-\phi} = 1 + \left[\cos(\alpha_0) + 2\sqrt{Y_i - \sin\alpha_0}\sqrt{\tilde{E}Fr - Y_i}\right]\partial_{Y_i}\Delta\phi.$$

Therefore, the stability of the apex return map depends on the variation of the angle swept during stance with respect to the apex height y_i or the normalized apex height Y_i at stride i:

$$\partial_i\Delta\phi^* := \frac{\partial}{\partial_{Y_i}}\Big|_{\Delta\phi=2\alpha_0-\phi}\Delta\phi.$$

In normalized coordinates, this is given by

$$\begin{aligned}\partial_i\Delta\phi = {} & \frac{\sqrt{2}\tilde{k}}{\sqrt{Fr}(\tilde{k}+3)^{3/2}}\left\{\arccos\left(\frac{(1-\sin\alpha_0/Fr)}{\sqrt{(1-\sin\alpha_0/Fr)^2 + (\tilde{k}+3)[2\tilde{E} - 1 - 2\sin\alpha_0/Fr]}}\right)\right\}\times \\ & \left(\cos\alpha_0\frac{1}{\sqrt{Y_i - \sin\alpha_0}} + \sin\alpha_0\frac{1}{\sqrt{\tilde{E}Fr - Y_i}}\right) \\ & - \left\{\frac{\sqrt{2}}{\sqrt{Fr}(\tilde{k}+3)^{3/2}}\frac{[2(\tilde{k}+3) - 3(1-\sin\alpha_0/Fr)]\sqrt{\tilde{k}+3}\sqrt{2\tilde{E} - 1 - 2\sin\alpha_0/Fr}}{(1-\sin\alpha_0/Fr)^2 + (\tilde{k}+3)[2\tilde{E} - 1 - 2\sin\alpha_0/Fr]}\right\}\times \\ & \left(\cos\alpha_0\frac{1}{\sqrt{Y_i - \sin\alpha_0}} + \sin\alpha_0\frac{1}{\sqrt{\tilde{E}Fr - Y_i}}\right).\end{aligned} \tag{9}$$

See Appendix A.4 for the detailed deduction of this formula.

3. Results

Section 3.1 outlines the main features of the dataset analyzed; the verification of the validity of the hypothesis of approximate linearity of the angular dynamics during stance and numerics that confirm the accuracy of our approximation of both the radial and angular dynamics are discussed in Section 3.2; some examples of parameters which allow a symmetric stance phase are given in Section 3.3.

3.1. Human running data

For this paper, we used the publicly available dataset from Fukuchi et al. (2017). The dataset includes the time series of the three-dimensional coordinates of markers collected from sensors placed on the bodies of participants of an experiment which involved individuals running on a treadmill at three different velocities (2.5 m/s, 3.5 m/s, and 4.5 m/s). The data was collected with a motion-capture system and includes kinematics, kinetics, and biometrics, such as age and mass of the individual, of 28 human subjects. For our analysis, we considered only sagittal plane data.

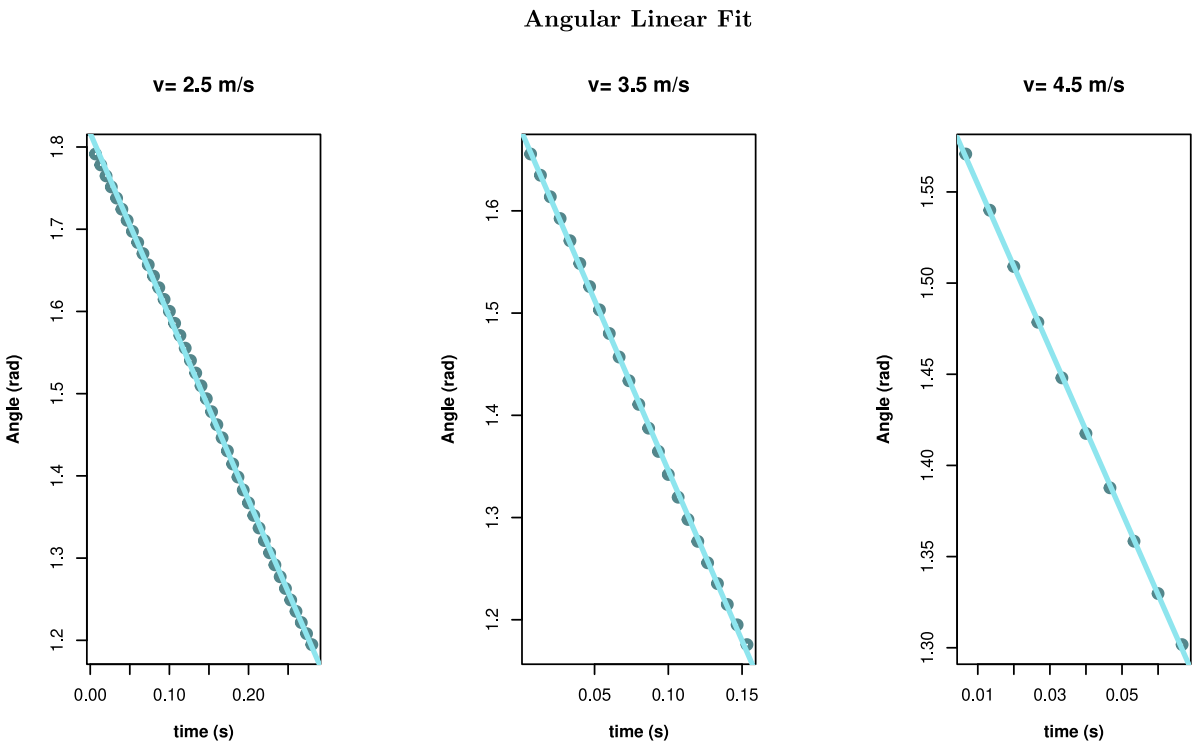

Fig. 2. Angular linear fit - Subject 1 - Stride 1. The x-axis represents the time t. The y-axis represents the angle ϕ during stance. Left Plot: At velocity $v = 2.5$ m/s, we have $\hat{\omega} = -2.23$ and adjusted $R^2 = 0.9993$. Central Plot: At velocity $v = 3.5$ m/s, we have $\hat{\omega} = -3.33$ and adjusted $R^2 = 0.9996$. Right Plot: At velocity $v = 4.5$ m/s, we have $\hat{\omega} = -4.45$ and adjusted $R^2 = 0.9997$. All p-values are < 0.001.

Before starting the analysis, we pre-processed the data in the same way as we did in Selvitella and Foster (2023). In particular: we divided the strides and extracted the stance phases, where our approximation is non-trivial (See Section 2.1); we paired kinematic and kinetic data so as to have the values of those measurements with the same frequency, and we calculated the CoM sagittal coordinates by averaging the left and right markers that were closest to the estimated position of the CoM, namely the sagittal coordinates of the *anterior superior Iliac spine*, the *posterior Iliac spine*, and the *Iliac crest*. Given that the coordinate system of the time series in Fukuchi et al. (2017) was centered at an origin static with respect to the treadmill, we performed a Galilean transformation to recenter the data: $x' = x + vt, y' = y + vt$ with (x, y) the coordinates with respect to the treadmill origin, t the time, and v the velocity of the treadmill in that trial. Three different velocities were considered: $v = 2.5$ m/s, $v = 3.5$ m/s, and $v = 4.5$ m/s. For more information, please refer to Fukuchi et al. (2017) and Selvitella and Foster (2023).

3.2. Validity of the hypothesis of our approximation

3.2.1. Constant angular velocity

Our approximation of the SLIP dynamics assumes that $\dot{\phi} = \omega < 0$. Here, we demonstrate empirically, using the data from Fukuchi et al. (2017), that this assumption is reasonable. To do so, we fitted a linear model of the form: $\phi = \phi_0 + \dot{\phi}_0 t + \epsilon$, with ϵ an error term. Using ordinary least squares, we obtain $\hat{\phi}_0 = \bar{\dot{\phi}}_0$. We used this as an estimate for ω: $\hat{\omega} = \bar{\dot{\phi}}_0$. We tested this model for Stride 1 of Subject 1 in Fukuchi et al. (2017). We fitted a separate model for each of the three velocities $v = 2.5$ m/s, $v = 3.5$ m/s, and $v = 4.5$ m/s. We tested for normality of the angular variable ϕ in the three conditions using the Shapiro–Wilk Normality Test. The test was performed at level $\alpha = 0.05$. The test failed to reject the null hypothesis H_0 of normality in all three conditions The p-values were $p = 0.06064$, $p = 0.3435$, $p = 0.8788$ for the three conditions $v = 2.5$ m/s, $v = 3.5$ m/s, $v = 4.5$ m/s, respectively. Furthermore, we fitted a linear regression model and tested for $H_0 : \dot{\phi}_0 = 0$ vs. $H_A : \dot{\phi}_0 \neq 0$ with a two sided t-test. The model fit is visualized in Fig. 2. All models demonstrated a good fit ($p-$value < 0.001 and adjusted $R^2 > 99.9\%$ for all the models).

As a consequence, the prediction of the angle swept during stance is also accurate using our approximation. We checked this by multiplying the observed stance duration time ΔT with $\hat{\omega}$ and by checking the accuracy of $\widehat{\Delta\phi} := \Delta T * \hat{\omega}$ as a predictor of the correct $\Delta\phi$. Again, we tested for normality of the angle swept during stance $\Delta\phi$ in the three conditions using the Shapiro–Wilk Normality Test. The test was performed at level $\alpha = 0.05$. The test failed to reject the null hypothesis H_0 of normality in all three conditions. The p-values were $p = 0.8488$, $p = 0.4481$, $p = 0.05871$ for the three conditions $v = 2.5$ m/s, $v = 3.5$ m/s, $v = 4.5$ m/s, respectively. We report that for the condition $v = 4.5$ m/s, excluding only the first stride provides a significant difference from normality with the same test. We used all consecutive strides of Subject 1 in the three conditions $v = 2.5$ m/s, $v = 3.5$ m/s, $v = 4.5$ m/s, excluding the first two strides of the sequence (typically considered outliers and subject to noise). We fitted linear regression models of the form $\Delta\phi$ vs. $\widehat{\Delta\phi}$ and tested for significance with a two sided t-test. All models demonstrated a good fit ($p-$value < 0.001 and adjusted $R^2 > 99.9\%$ for all the models). This model fit is visualized in Fig. 3. For more details, we refer to Appendix A.6.

3.2.2. Radial and angular approximation vs. numerical integration

In this subsection, we check how well the radial variable of our model r_a approximates that of the full SLIP, solved numerically, r_n and how well the angular variable of our model ϕ_a approximates the numerical one ϕ_n. The numerical approximation of the SLIP model is performed using

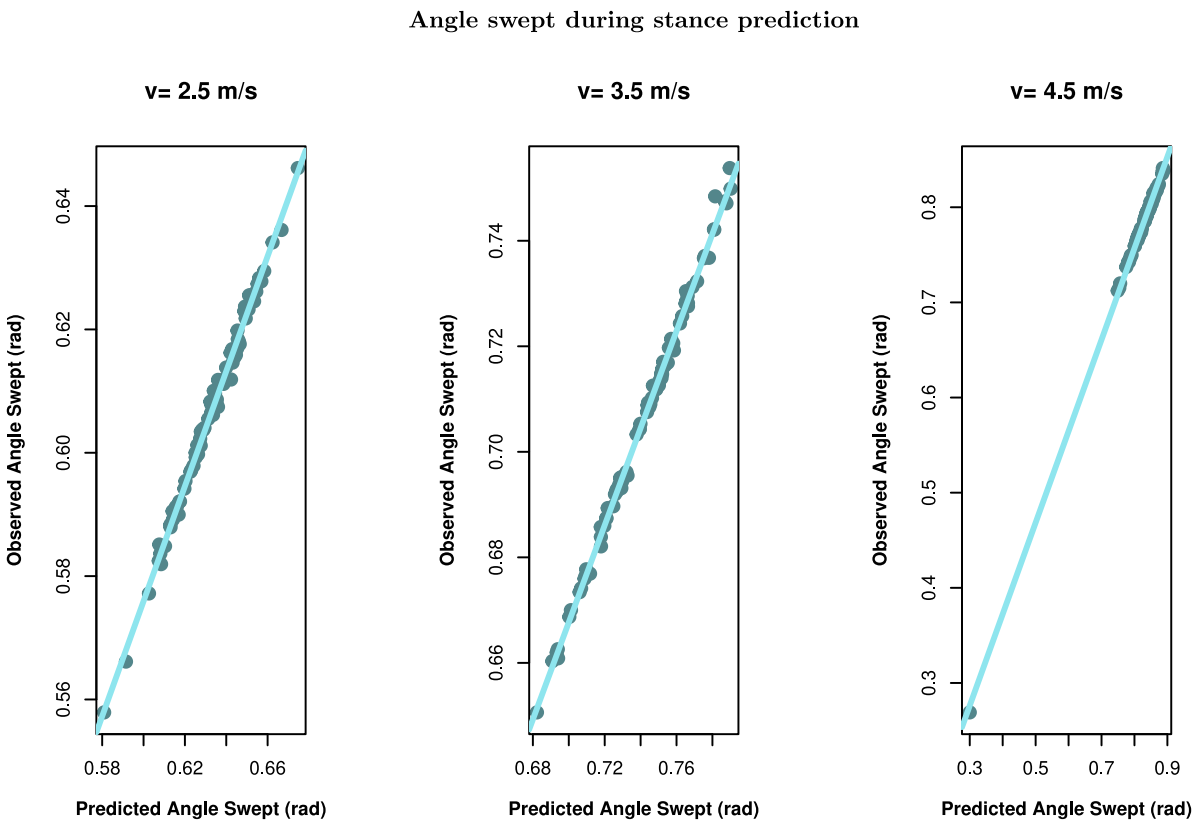

Fig. 3. Angle swept during stance - Subject 1. The x-axis represents $\widehat{\Delta\phi}$. The y-axis represents $\Delta\phi$. Left Plot: At velocity $v = 2.5$ m/s, we have adjusted $R^2 = 0.9946$. Central Plot: At velocity $v = 3.5$ m/s, we have adjusted $R^2 = 0.9972$. Right Plot: At velocity $v = 4.5$ m/s, we have adjusted $R^2 = 0.9988$. All p-values are < 0.001.

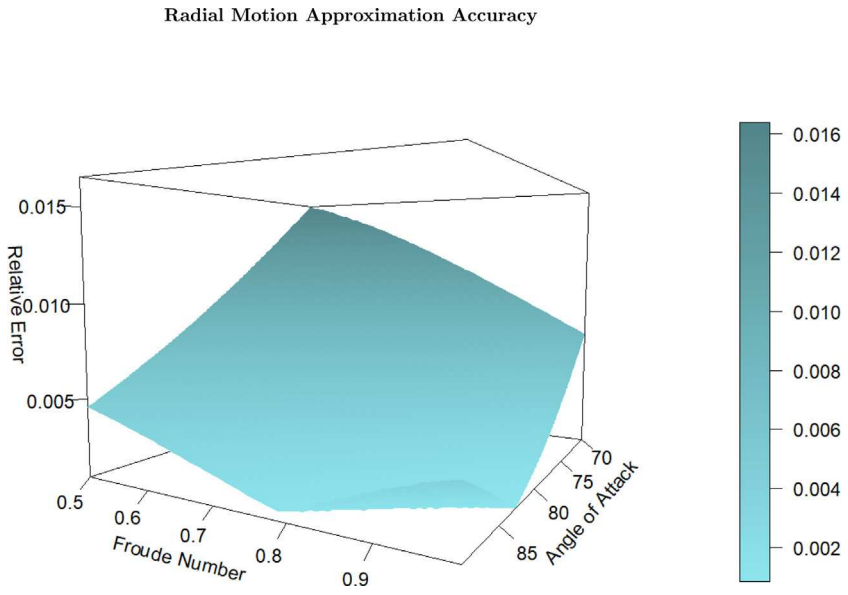

Fig. 4. Radial motion approximation accuracy. *Froude number*: $Fr \in [0.5, 0.995]$; Angle of attack $\alpha_0 \in [70 \text{ deg}, 89 \text{ deg}]$. These plots show the relative error (e_{rel}) of the radial distance of the CoM for our approximation r_a vs. the numerical solution r_n. Higher errors are colored darker as depicted in the color bar. In these experiments, $m = 80$ kg, $l_0 = 1$ m, $k = 16000$ N/m, and $E = 1200$ J.

the function *ode*, with integrator *lsoda*, from the *R* software package *deSolve*. We measure the distance between r_a and r_n in terms of the relative error e_{rel} of the L^∞ norm:

$$e_{rel} := \frac{\|r_a(t) - r_n(t)\|_{L^\infty[t_{TD}, t_{TO}]}}{\|r_n(t)\|_{L^\infty[t_{TD}, t_{TO}]}},$$

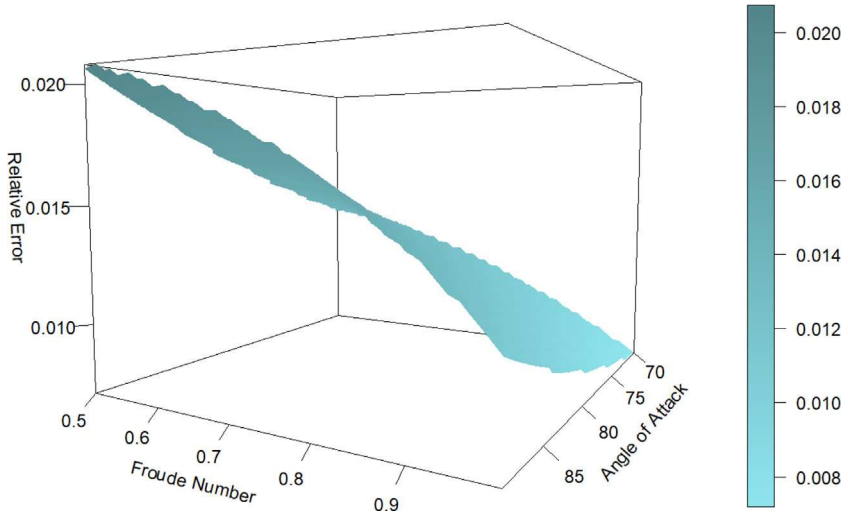

Fig. 5. Angular motion approximation accuracy. *Froude number*: $Fr \in [0.5, 0.995]$; Angle of attack $\alpha_0 \in [70 \text{ deg}, 89 \text{ deg}]$. These plots show the relative error (e_{rel}) of the angular distance of the CoM for our approximation ϕ_a vs. the numerical solution ϕ_n. Higher errors are colored darker as depicted in the color bar. In these experiments, $m = 80$ kg, $l_0 = 1$ m, $k = 16000$ N/m, and $E = 1200$ J.

where $\|f(t)\|_{L^\infty[a,b]} := \sup_{t\in[a,b]} |f(t)|$, as in Selvitella and Foster (2022b). Analogously, we measure the distance between ϕ_a (our approximation) and ϕ_n (numerical integration) of the angular variable:

$$e_{rel} := \frac{\|\phi_a(t) - \phi_n(t)\|_{L^\infty[t_{TD},t_{TO}]}}{\|\phi_n(t)\|_{L^\infty[t_{TD},t_{TO}]}},$$

In all these experiments, we use the parameters $m = 80$ kg, $l_0 = 1$ m, $k = 16000$ N/m, and $E = 1200$ J. In Fig. 4, we show the values of e_{rel} for the radial variable for parameters $Fr \in [\ 0.5,\ 0.995]$ and $\alpha_0 \in [70 \text{ deg}, 89 \text{ deg}]$. As shown in Fig. 4, the errors e_{rel} are all between 0.14 % ($Fr = 0.95$, $\alpha_0 = 85$ deg) and 1.65 % ($Fr = 0.5$, $\alpha_0 = 70$ deg). In Fig. 5, we show the values of e_{rel} for the same sets of parameters but for the angular variable. As shown in Fig. 5, the errors e_{rel} are all between 0.68 % ($Fr = 0.995$, $\alpha_0 = 70$ deg) and 2.06 % ($Fr = 0.5$, $\alpha_0 = 89$ deg). Some analytical deductions on the effect of our approximation to the error made in the potential energy are also possible. If, for the purpose of this computation, we denote the exact potential energy by E_{pot} and the approximate one by $\tilde{E}_{pot}$, we have

$$|E_{pot} - \tilde{E}_{pot}| = mgr|\sin(\phi) - \sin(\alpha_0)| = mgr|\sin(\alpha_0) + (\phi - \alpha_0)\cos(\alpha_0) + o(\phi - \alpha_0)| \leq mgl_0|\phi - \alpha_0| + o(\phi - \alpha_0)$$

and so the error made in the potential energy is of first order in the assumption of small angle swept during stance. Therefore, if we measure the relative error made by $\tilde{E}_{pot}$ in approximating E_{pot} by

$$e_{rel,pot} := \frac{\|E_{pot} - \tilde{E}_{pot}\|_{L^\infty[t_{TD},t_{TO}]}}{mgl_0},$$

we obtain that

$$e_{rel,pot} \leq C|\phi - \alpha_0| \leq C\Delta\phi.$$

This implies that the error made in the potential energy is small under our assumption of small angle swept during stance and it can be directly bounded by our approximation, following the analysis in Appendix A.5.

3.3. Existence of solutions with symmetric stance phase

For symmetric contacts, we have $\Delta\phi = 2\alpha_0 - \pi$ and so Eq. (3) implies

$$2\alpha_0 - \pi = -\frac{2}{\sqrt{\tilde{k}+3}} \arccos\left\{ \frac{1 - \sin\alpha_0/Fr}{\sqrt{(1-\sin\alpha_0/Fr)^2 + (\tilde{k}+3)(2\tilde{E} - 1 - 2\sin\alpha_0/Fr)}} \right\}. \tag{10}$$

Given that this equation is highly nonlinear, it is legitimate to wonder if there are combinations of the parameters (α_0, E, k, and Fr) or, equivalently, of their normalized versions, which allow for the existence of solutions. Below are some explicit examples.

Example A. Consider $\alpha_0 = 85$ deg and $\tilde{E} = 2.51$, $l_0 = 1$ m, $m = 80$ kg, and $\omega^2 = 0.5 * g/l_0$ ($Fr = 0.5$), then $\tilde{k} = 25.5817$ and so $k = \tilde{k}m\omega^2 = 24.09064 * 80 * 9.8 = 18906.33$.

Example B. Consider $\alpha_0 = 87.5$ deg and $\tilde{E} = 1.8$, $l_0 = 1.2$ m, $m = 85$ kg, and $\omega^2 = 0.9 * g/l_0$ ($Fr = 0.9$), then $\tilde{k} = 33.67553$ and so $k = \tilde{k}m\omega^2 = 33.67553 * 85 * 9.8/1.2 = 23400.28$.

Example C. Consider $k = 20000$ and $\tilde{E} = 2.51$, $l_0 = 1$ m, $m = 80$ kg, and $\omega^2 = 0.995g/l_0$ ($Fr = 0.995$), then $\tilde{k} = 25.51$ and so $\alpha_0 = 86.84229$ deg.

Example D. Consider $k = 16000$ and $\tilde{E} = 2.2$, $l_0 = 1.1$ m, $m = 85$ kg, and $\omega^2 = 0.95g/l_0$ ($Fr = 0.995$), then $\tilde{k} = 21.10691$ and so $\alpha_0 = 86.24524$ deg.

Example E. Consider $\alpha_0 = 90$ deg, $\tilde{k} = 24$ and $Fr = 0.5$. Then $\tilde{E} = 2.49$ and so $2\tilde{E} - 1 - 2\sin\alpha_0/Fr < 0$, which is not in the admissible range since $\nu > 0$.

These examples do not exhaust the set of parameters under which solutions to Eq. (10) exist or do not exist. As mentioned, we cannot expect explicit formulas in terms of elementary functions and we believe that the implicit formula (10), although complex, is the most concise and useful to illustrate the relationship among those parameters α_0, E, k, and Fr that give rise to a symmetrical stance phase. As emerges from Examples A to E, even small differences in the parameter ranges can give rise to different types of solutions. Parameters which belong to the inadmissible set (no symmetric stance phase possible) are parameters for which our approximation predicts that the contact phase cannot be exactly symmetric, while the set of admissible parameters (those that provide a solution to Eq. (10)) support the possibility of symmetric stance phases for the SLIP dynamics. The parameters in the examples have been chosen to try to cover several possible behaviors. Examples A to D, those with admissible parameters, have a *Froude number* increasing (while going from Examples A to D) towards 1, which is the case covered in Geyer et al. (2005) and relates to the typical trotting speed of horses and jogging speed of human (Alexander, 1989). Example E covers the extreme case of vertical touch-down angle and, as expected, does not permit an admissible combination of parameters. The threshold for admissibility is a complicated codimension one manifold.

4. Discussion

4.1. Main features of our approximation

One of the novelties of our result is the derivation of a condition for the asymptotic stability of periodic orbits of the SLIP model (1) that is valid without restrictions on the range of parameters. In Geyer et al. (2005), the authors assumed that $a = 0$, or equivalently $\omega = -\sqrt{g/l_0}$ or $Fr = 1$, while our condition for stability is valid for all $Fr > 0$. On the other side, we use a lower order approximation of the angular dynamics. In Geyer et al. (2005), authors approximated the SLIP angular dynamics $\dot{\phi} = \omega(1+\rho^2)^{-1} \simeq \omega * (1+2|\rho|)$, which is theoretically more accurate than ours: $\dot{\phi} \simeq \omega$. The gain obtained using a 1-st order instead of a 0-th order approximation is small, as the accuracy only increases of a factor $\rho \ll 1$. Moreover, the lower order approximation that we performed did not have too much of an effect on the accuracy of the fit for the data that we analyzed, as demonstrated in Section 3.2. We have traded a little bit of accuracy by cutting out an oscillating component from the angle swept during stance, to gain extra interpretability (a 1d linear model is probably the most interpretable among the non-constant models) and a lot of information about the stability structure of periodic orbits of the SLIP model. Note that ours are the simplest biologically meaningful assumptions for the angular dynamics. Indeed, simplifying to $\phi = \pi/2$ would imply that the dynamics reduces to the 1d dynamics of hopping on the spot (instead of the 2d dynamics of running), while assuming $\phi = c \neq \pi/2$ would make the model biologically unreasonable. Again, the simplest non-constant motion is that with constant velocity $\dot{\phi} \simeq \omega$. For what concerns the radial dynamics, Blickhan and Full (1993) showed that the relative leg compression is of order $\rho \sim 10^{-1}$ for almost all animals, humans included, and so the assumption $\rho \ll 1$ might not look quite right. To compensate for this, at least in part, we keep higher order terms in ρ in the expansion of the angular momentum: $(1+\rho)^{-2} \simeq 1 - 2\rho + 3\rho^2$. For further comments about the favorable/compensating behavior of the approximate SLIP dynamics, we refer to Geyer et al. (2005).

Even if our approximation is simpler than that in Geyer et al. (2005), it shows a very high adjusted R^2 (> 0.993), and so adding further terms can improve the fit of no more than 1%, as measured by the adjusted R^2. The very good fit of our approximation is reflected also in the accuracy of the approximation of the angle swept during stance. This is extremely important, as this quantity is the only quantity that depends on the SLIP stance dynamics that appears explicitly in the apex return map. Note that the stability condition is satisfied in an open set of parameters and so parameters close to parameters which give rise to stable solutions give rise to stable solutions as well. Our approximate solution compares well with the numerical solutions, as depicted in Figs. 4 and 5, and produces an accurate approximate apex return map (See Appendix A.5); therefore, our approximation predicts a set of parameters for which the true solution is stable with minimal loss in accuracy.

Although we have a closed form representation of the approximate angular and radial dynamics which includes the effect of gravity g, and we derive an explicit condition for the asymptotic stability of periodic running gaits, the condition for stability is quite involved and tedious to derive (See Appendix). In fact, the condition for stability still depends on a relatively high-dimensional set of parameters (k, α_0, E, Fr). Note that, although we did not investigate the dependency structure among the parameters, we expect that such a dependency structure is indeed present and that, exploiting it in full, might simplify the stability analysis. The Christmas Candy Cane-shaped curve that bounds the stability region of the apex return map is quite narrow (see Fig. 7), and so it is not easy to guess which parameters produce asymptotically stable orbits and which do not simply by looking at the stability condition. Speculatively, this might be interpreted as a deficiency of spring–mass models which cannot fully capture, in such a reductionist form, the capacity of animals to run in a stable manner under many different perturbations.

The dataset that we analyzed has been kindly made publicly available by the authors of Fukuchi et al. (2017). We want to emphasize the importance that publicly available data and open access can have for encouraging both the possibility of interactions between labs and the development of cutting edge methodology aimed to combine data collected in different sites or under different conditions (Delp, 2023; Foster and Selvitella, 2022b,a, 2020).

4.2. A bifurcation phenomenon driven by the Froude number

The appearance of the extra parameter Fr in our approximation gives rise to an interesting bifurcation phenomenon. To illustrate this, we consider the same critical point of the apex return map considered in Geyer et al. (2005), namely that with height $Y^* = 0.8715324$. We also obtain that, for $Fr = 1$ (the only regime considered in Geyer et al. (2005)), the corresponding periodic trajectory is asymptotically stable. In addition, our analysis numerically determined that asymptotic stability persists for $Fr \in [0.85, 1]$, while it is lost outside this range. The situation is described in Fig. 6, where the dependency on the normalized energy $\tilde{E}$ of the stability of Y^* is also considered. Note that the range of values of Fr and E (e.g. $\tilde{E} = 1.77$ corresponds to $E = 1180$ J) considered here for the stability of the running gait are reasonable for human running.

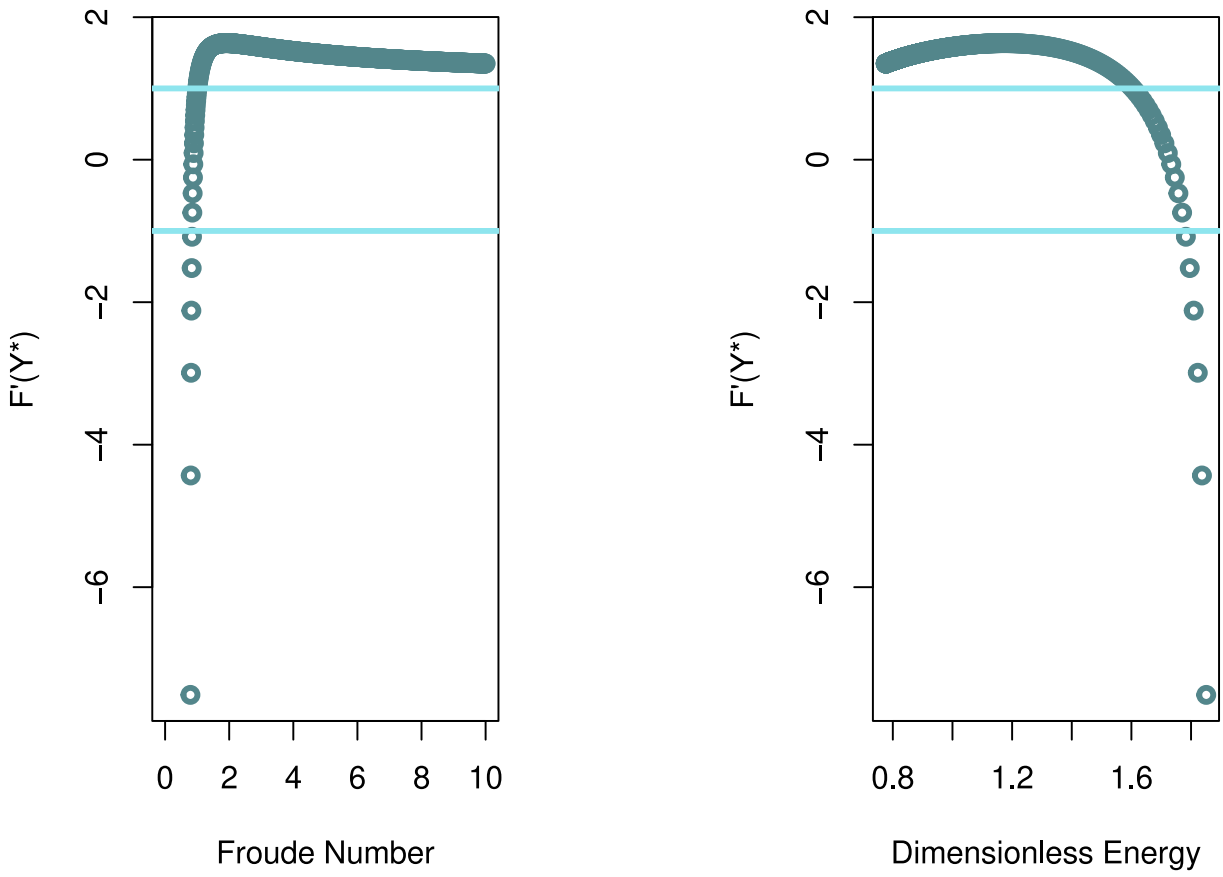

Fig. 6. Bifurcation diagram. The y-axis represents $F'(Y*) := \frac{\partial}{\partial Y_i}|_{Y=Y^*} F(Y)$ with $Y^* = 0.871532$. The two horizontal lines are at values $-1, +1$, the stability boundary. Left Plot: The x-axis represents the *Froude number* Fr. Y^* is stable only for $Fr \in [0.85, 1]$. Right Plot: The x-axis represents the dimensionless energy $\tilde{E}$. Y^* is stable only for $\tilde{E} \in [1.61, 1.77]$.

4.3. Asymmetric stance phase?

The analysis of stability reported in this paper assumes symmetric stance phases ($\Delta\phi = 2\alpha_0 - \pi$). One of the advantages of assuming this type of symmetry, is that such a condition simplifies the study of fixed points of the apex return map. In particular, the assumption $\Delta\phi = 2\alpha_0 - \pi$ is convenient because, given the chain of maps

$$(Y_i|\tilde{k}, Fr, \alpha_0, \tilde{E}) \quad \mapsto \quad (\Delta\phi, Y_i|\tilde{k}, Fr, \alpha_0, \tilde{E}) \quad \mapsto \quad F(Y_i|\tilde{k}, Fr, \alpha_0, \tilde{E})$$

in which we can decompose the apex return map $Y_i \mapsto F(Y_i|\tilde{k}, Fr, \alpha_0, \tilde{E})$, the assumption $\Delta\phi = 2\alpha_0 - \pi$ makes the second of the two maps in the chain equal to the identity map.

As noted in Geyer et al. (2005), for asymmetric contact phases, the energy conservation is violated, since $\Delta E_{pot} = mg(y_{TO} - y_{TD}) \neq 0$. Although confidence in the necessity of symmetry of the contact phase emerged in Geyer et al. (2005), we were not able to find in the literature the rigorous proof that such a midstance symmetry is a necessary condition for stable gaits in the SLIP model. Given that, in fact, running does not have exactly symmetric stance phases in the sagittal plane, a model extension is probably needed if we want to study asymmetric gaits in more detail. In fact, a series of papers, including (Yu et al., 2012; Kilic and Braun, 2023; Shahbazi et al., 2016), concerning novel, but more complex, approximations to the SLIP model that are particularly relevant to the case of asymmetric stance phases, have appeared in the literature with the intent of understanding the strengths and weaknesses of the SLIP dynamics without the assumption of symmetry around mid-stance. We commented on this in the introduction, where we compared these models with our approximation.

Recall that it is well known that certain animals, such as horses, prefer asymmetric gaits, such as galloping, when they increase their velocity during forward locomotion (Alexander, 2003b,a, 1984). The asymmetry of galloping at high *Froude number* is more evident in the horizontal plane and is different from the asymmetry of the CoM trajectory with respect to midstance that we are discussing here. Still, it is interesting to see the emergence of asymmetry in different versions for high-speed forward locomotion gaits.

The apex return map depends explicitly on the stance dynamics only through $\Delta\phi$ (See Eq. (9)). If we forget for an instant that we are considering a specific differential equation during stance and if we assign carefully chosen values to $\Delta\phi$, we have a plethora of possible different behaviors for the fixed points of the apex return map. In Fig. 7, we show two examples (and corresponding versions zoomed in around the fixed point of the apex return map) of parameters which lead to stable dynamics. Instead, in Fig. 8, we show an example of a fixed point with unstable dynamics (left) and another example with stable, but biologically unreasonable, dynamics (very large stiffness/non-compliant leg). Again, in these examples, we do not deduce $\Delta\phi$ from the SLIP model, but we fix it as a parameter.

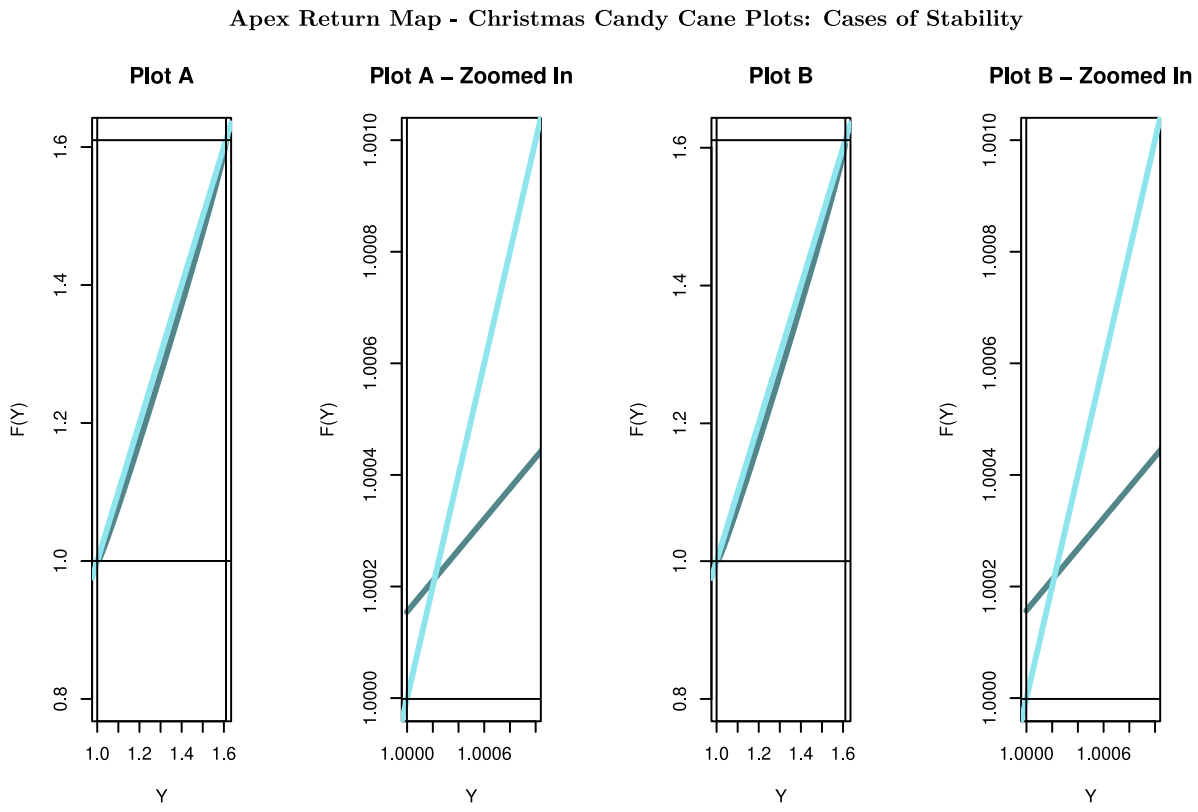

Fig. 7. Apex return map - Stability. The x-axis represents Y_i. The y-axis represents Y_{i+1}. The vertical and horizontal lines represent the boundary of validity of formula (8) ($\tilde{E}Fr \geq Y_i \geq \sin\alpha_0$). The plots in the full parameter range are accompanied by zoomed in versions around the fixed point of the apex return map. The plots show the characteristic Christmas Candy Cane shape. We assumed $m = 80$ kg and $l_0 = 1$ m. Left Plots (Plot A and Plot A - Zoomed In): $Fr = 1$, $\tilde{E} = 1.61$, $\alpha_0 = 89.9$ deg, $\Delta\phi = -0.05$ rad, and so $\alpha_0 - \Delta\phi \simeq 93$ deg $\neq \pi - \alpha_0$. Right Plots (Plot B and Plot B - Zoomed In): $Fr = 1.1$, $\tilde{E} = 1.81$, $\alpha_0 = 89.9$ deg, $\Delta\phi = -0.04$ rad, and so $\alpha_0 - \Delta\phi \simeq 92$ deg $\neq \pi - \alpha_0$. In these plots, the light blue curves represent the line $Y_{i+1} = Y_i$, while the dark blue curves represent the apex return map $Y_{i+1} = F(Y_i)$.

4.4. Further considerations

We have shown that the regime of constant angular velocity during stance leads to explicit formulas in the full range of parameters of the SLIP model. We have successfully tested this hypothesis on publicly available data from experiments of humans running on a treadmill at different velocities (Fukuchi et al., 2017). However, given the novelty and potential importance of our findings, it would be interesting to test our hypotheses in more general settings and verify to what extent our model has biological applicability. It is actually hard to have complete information on the biological relevance of the hypotheses of a mathematical model of locomotion. Note that, in Geyer et al. (2005), authors do not fully analyze human data to test their model, but evaluate the accuracy of the predictions of their approximations using parameters relevant to humans (page 323 of Geyer et al. (2005)) and scrutinize the applicability of their assumptions.

We do not know how well our approximations perform in the case of running on the ground. It has been reported that these two conditions (ground vs treadmill) are comparable, but there might be sagittal plane kinematic differences at footstrike (Hooren et al., 2020). It would also be good to test our approximations with experiments of humans running on uneven or rough terrains. We do not have full information about the applicability of our assumptions outside the range of velocities considered (lower than $v = 2.5$ m/s or higher than $v = 4.5$ m/s). We can expect that our hypotheses are challenged in the case of sprinting or other cases in which the angle of attack is particularly low and the angle swept during stance is large. Testing the hypotheses of constant angular velocity during stance in these cases would be interesting. In our experiments, we showed that the dynamics in the regime of constant angular velocity during stance approximates both radial and angular SLIP motions well for angles of attack as low as 70 deg, which is beyond what can be reasonably considered a small deflection from the vertical position. Still, caution needs to be taken in using the constant angular velocity approximation (and our other hypotheses) for angles of attack departing substantially from 90 deg.

As mentioned in the introduction, research has shown that the SLIP model captures the sagittal dynamics of animals, such as cockroaches, dogs, kangaroos, and birds (Full and Koditschek, 1999) and that spring–mass models accurately predict energetics in many locomotor gaits (Blickhan and Full, 1993; Dickinson et al., 2000). The performance of our approximation in species other than humans is an interesting question that we are not addressing in this paper.

5. Conclusions

In this paper, we developed an approximation of the SLIP model for running with the simplest possible non-trivial angular dynamics, namely that with constant angular velocity. In the case of small compression and of small angle swept during stance, we proved, using publicly available human running data, the validity of the assumptions of constant angular velocity and we demonstrated the accuracy of our approximation of the SLIP radial and angular dynamics. Furthermore, we provided explicit conditions for the asymptotic stability of periodic running gaits in the full

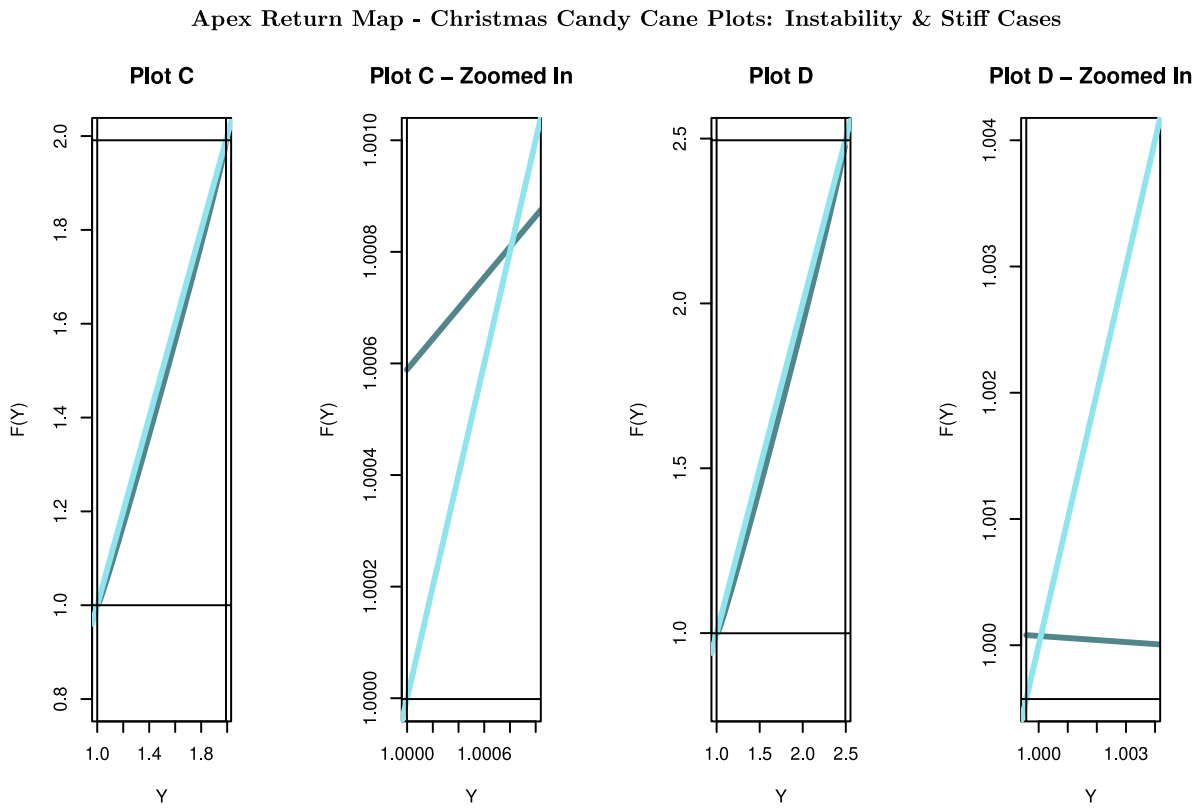

Fig. 8. Apex return map - Instability & Biologically unmeaningful cases. The x-axis represents Y_i. The y-axis represents Y_{i+1}. The vertical and horizontal lines represent the boundary of validity of formula (8) ($\tilde{E}Fr \geq Y_i \geq \sin\alpha_0$). The plots in the full parameter range are accompanied by zoomed in versions around the fixed point of the apex return map. The plots show the characteristic Christmas Candy Cane shape. We assumed $l_0 = 1.1$ m. Left Plots (Plot C and Plot C - Zoomed In): $m = 70$ kg, $Fr = 1.1$, $\tilde{E} = 1.7$, $\alpha_0 = 87.5$ deg, $\Delta\phi = -0.6$ rad, and so $\alpha_0 - \Delta\phi \simeq 58$ deg $\neq \pi - \alpha_0$. ($k = 17825$ N/m). Right Plots (Plot D and Plot D - Zoomed In): $m = 80$ kg, $Fr = 0.69$, $\tilde{E} = 3.6157$, $\alpha_0 = \pi - 1.6$ rad, $\Delta\phi = -0.1$ rad, and so $\alpha_0 - \Delta\phi \simeq 94$ deg $\neq \pi - \alpha_0$ ($k > 500{,}000$ N/m). In this plot, the light blue curves represent the line $Y_{i+1} = Y_i$, while the dark blue curves represent the apex return map $Y_{i+1} = F(Y_i)$.

range of parameters and illustrated the emergence of bifurcation phenomena when we vary the *Froude number*: stable gaits can become unstable when the *Froude number* parameter is outside a certain range. Furthermore, our analysis highlights the need for a deeper understanding of models which admit periodic gaits that are asymmetric with respect to midstance as well as a complete mathematical explanation of the transitions from symmetric to asymmetric gaits at high speeds and of the bifurcation phenomenon that we discussed in this paper.

CRediT authorship contribution statement

Alessandro Maria Selvitella: Writing – review & editing, Writing – original draft, Visualization, Validation, Supervision, Software, Resources, Project administration, Methodology, Funding acquisition, Formal analysis, Conceptualization. **Kathleen Lois Foster:** Writing – review & editing, Investigation, Funding acquisition, Conceptualization.

Declaration of competing interest

none.

Acknowledgments

AMS and KLF are supported by the collaborative U.S. National Science Foundation Awards # 2152789 and # 2152792 on *RUI: Collaborative Research: DMS/NIGMS 1: The mathematical laws of morphology and biomechanics through ontogeny* and by the NSF-Simons Center for Quantitative Biology - Northwestern University Pilot Project Grant on *On the mathematical and physical laws of the morphology and biomechanics of mourning geckos through ontogeny*. This paper is dedicated to Nonno Nunzio and to his great-grandson Nunzio Stanley.

Appendix

In this appendix, we will go through some technical details that lead to the main formulas derived from our approximation. Appendix A.1 includes the mathematical deductions needed to find the formula for the angle swept during stance, while Appendix A.2 derives the apex return map. In Appendix A.3, we derive the explicit formula for the fixed point of the apex return map as a function of α_0, Fr, and $\tilde{E}$. Appendix A.4 is devoted to the proof of the stability condition for periodic gaits under the assumption of our approximation of the SLIP dynamics. Appendix A.5 deduces rigorous error bounds for the approximate apex return map and includes heat maps for the accuracy of our approximation for a large set of values of the angle of attack and the Froude number. Appendix A.6 is dedicated to some extra data analysis. Appendix A.7 is devoted to a point-by-point comparison of our model with that of Geyer et al. (2005).

A.1. Proof of the formula for the angle swept during stance

In this subsection, we prove formula (3). By imposing the boundary conditions $r(t_{TD}) = r(t_{TO}) = l_0$ and inverting formula (2), we find that the times t_{TD} and t_{TO} are

$$t_{TD} = \frac{1}{\hat{\omega}_0}\left\{\left(2n+\frac{3}{2}\right)\pi - \left[\frac{\pi}{2} + \arcsin\left(-\frac{a}{b}\right)\right]\right\}, \quad t_{TO} = \frac{1}{\hat{\omega}_0}\left\{\left(2n+\frac{3}{2}\right)\pi + \left[\frac{\pi}{2} + \arcsin\left(-\frac{a}{b}\right)\right]\right\},$$

with $n \in \mathbb{Z}$. By integrating $\dot{\phi}$ from t_{TD} to t_{TO}, we find

$$\Delta\phi = \int_{t_{TD}}^{t_{TO}} \dot{\phi} dt = \int_{t_{TD}}^{t_{TO}} \omega dt = \omega(t_{TO} - t_{TD}) = \frac{\omega}{\hat{\omega}_0}\left\{\pi + 2\arcsin\left(-\frac{a}{b}\right)\right\}.$$

Simplifying further, by using the trigonometric formula $\pi + 2\arcsin -x = 2\arccos x$, we obtain

$$\Delta\phi = 2\frac{\omega}{\hat{\omega}_0}\left\{\arccos\left(\frac{a}{b}\right)\right\}.$$

By rescaling to the normalized variables

$$k = \tilde{k}m\omega^2, \quad \omega_0^2 = \tilde{k}\omega^2 \quad \hat{\omega}_0^2 = (\tilde{k}+3)\omega^2, \quad g/l_0 = \omega^2/Fr, \quad E = \tilde{E}ml_0^2\omega^2$$

and given that $\dot{\phi} = \omega < 0$ (negative, as we are concerned with forward locomotion only), we get

$$\Delta\phi(\tilde{k}, \alpha_0, \tilde{E}) = -\frac{2}{\sqrt{\tilde{k}+3}}\arccos\left\{\frac{1 - \sin\alpha_0/Fr}{\sqrt{(1-\sin\alpha_0/Fr)^2 + (\tilde{k}+3)(2\tilde{E} - 1 - 2\sin\alpha_0/Fr)}}\right\}.$$

A.2. Derivation of the apex return map

In this subsection, we derive the apex return map in Eq. (7). For the definitions of the maps in this derivation, please refer to Section 2.2.1. By conservation of energy at apex $i+1$ and take off TO, we have:

$$\frac{m}{2}\left(\dot{x}_{i+1}^2 + \dot{y}_{i+1}^2\right) + mgy_{i+1} = \frac{m}{2}\left(\dot{x}_{TO}^2 + \dot{y}_{TO}^2\right) + mgy_{TO}.$$

The motion from take off to the apex $i+1$ takes place only during the flight phase, during which, no horizontal force is present and so $\dot{x}_{i+1} = \dot{x}_{TO}$. Given that y_{i+1} is the apex during stance $i+1$, then $\dot{y}_{i+1} = 0$ (this is one of the reasons for choosing the apex return map as Poincaré map). Using this information, we obtain

$$mgy_{i+1} = \frac{m}{2}\dot{y}_{TO}^2 + mgy_{TO}$$

and so

$$y_{i+1} = y_{TO} + \frac{1}{2g}\dot{y}_{TO}^2.$$

This gives f_+. Using the change of variables T^{-1}: $x(t) = r(t)\cos(\phi(t))$; $y(t) = r(t)\sin(\phi(t))$, we obtain that during stance:

$$\dot{y} = \dot{r}(t)\cos(\phi(t)) + r(t)\dot{\phi}(t)\sin(\phi(t))$$

and so, at take off, we have

$$\dot{y}_{TO} = \dot{r}_{TO}\sin(\phi_{TO}) + r_{TO}\dot{\phi}_{TO}\cos(\phi_{TO}).$$

Using f_0, which is simply a consequence of our assumptions (e.g. take off and touch down happen with a straight leg; the definitions of take off and touch down; we are considering only forward motion), we obtain

$$\dot{y}_{TO} = -\dot{r}_{TD}\sin(\phi_{TD} + \Delta\phi) + l_0\dot{\phi}_{TD}\cos(\phi_{TD} + \Delta\phi).$$

Using the polar coordinates change of variables T to transform back to Euclidean coordinates, we obtain

$$\dot{y}_{TO} = -(\dot{x}_{TD}\cos\phi_{TD} + \dot{y}_{TD}\sin\phi_{TD})\sin(\phi_{TD} + \Delta\phi) + (\dot{y}_{TD}\cos(\phi_{TD}) - \dot{x}_{TD}\cos\phi_{TD})\cos(\phi_{TD} + \Delta\phi).$$

Using formulas for summation of angles, we simplify to

$$\dot{y}_{TO} = -\dot{x}_{TD}\sin(2\phi_{TD} + \Delta\phi) + \dot{y}_{TD}\cos(2\phi_{TD} + \Delta\phi).$$

By conservation of energy at apex of i, we have:

$$\frac{m}{2}\left(\dot{x}_i^2 + \dot{y}_i^2\right) + mgy_i = E,$$

which gives

$$\dot{x}_{TD} = \dot{x}_i = \sqrt{\frac{2}{m}(E - mgy_i)}.$$

This is true because the motion from apex i and the next touch down takes place only during the flight phase, during which, no horizontal force is present and so $\dot{x}_{TD} = \dot{x}_i$. Note also that at y_i, the apex during stance i, we have $\dot{y}_i = 0$. At touch down, we also have

$$y_{TD} = l_0\sin(\phi_{TD}) = l_0\sin(\pi - \alpha_0) = l_0\sin(\alpha_0).$$

By conservation of energy at apex i and touch-down TD, we have:

$$\frac{m}{2}\left(\dot{x}_i^2+\dot{y}_i^2\right)+mgy_i=\frac{m}{2}\left(\dot{x}_{TD}^2+\dot{y}_{TD}^2\right)+mgy_{TD},$$

which, with similar arguments to those used above, leads to $\dot{y}_{TD}=-\sqrt{2g(y_i-y_{TD})}=-\sqrt{2g(y_i-l_0\sin\alpha_0)}$. This gives f_-. Note that we used the positive root for the formula for $\dot{x}_i$ because we are concerned only with forward motion and we used the negative root for $\dot{y}_{TD}$ because, in order to touch down, the mass needs to move downward. By assumption, the angle of attack (touch down) is $\phi_{TD}=\pi-\alpha_0$. Using f_-, we obtain that

$$\dot{y}_{TO}=-\sqrt{\frac{2}{m}(E-mgy_i)}\sin(\Delta\phi-2\alpha_0)-\sqrt{2g(y_i-l_0\sin\alpha_0)}\cos(\Delta\phi-2\alpha_0).$$

Plugging this inside

$$y_{i+1}=y_{TO}+\frac{1}{2g}\dot{y}_{TO}^2,$$

and collecting a factor of $\sqrt{\frac{2}{m}}$, we obtain

$$y_{i+1}=f(y_i)=\frac{1}{mg}\left[\cos(\Delta\phi-2\alpha_0)\sqrt{mg(y_i-l_0\sin\alpha_0)}+\sin(\Delta\phi-2\alpha_0)\sqrt{E-mgy_i}\right]^2+l_0\sin(\alpha_0-\Delta\phi).$$

This completes the derivation of the formula for the apex return map (7).

A.3. Calculation of the fixed point of the apex return map

As shown in Geyer et al. (2005), the apex return map for the SLIP model takes the form:

$$y_{i+1}=f(y_i)=\frac{1}{mg}\left[\cos(\Delta\phi-2\alpha_0)\sqrt{mg(y_i-l_0\sin\alpha_0)}+\sin(\Delta\phi-2\alpha_0)\sqrt{E-mgy_i}\right]^2+l_0\sin(\alpha_0-\Delta\phi)$$

with the condition

$$y_{i+1}\geq l_0\sin(\alpha_0).$$

By rescaling $Y_i:=y_i/l_0$ and $F(Y_i):=f(y_i)/l_0$, we get

$$Y_{i+1}=F(Y_i)=\left[\cos(\Delta\phi-2\alpha_0)\sqrt{Y_i-\sin\alpha_0}+\sin(\Delta\phi-2\alpha_0)\sqrt{\tilde{E}Fr-Y_i}\right]^2+\sin(\alpha_0-\Delta\phi).$$

From equation (24) in Geyer et al. (2005) and under the assumptions of constant angular velocity and forward motion $\dot{\phi}=\omega<0$, we get

$$\omega=\sqrt{\frac{2g}{l_0}}\left(\cos\alpha_0\sqrt{Y_i-\sin\alpha_0}-\sin\alpha_0\sqrt{\tilde{E}Fr-Y_i}\right),$$

and so

$$-\sqrt{\frac{Fr}{2}}=\cos\alpha_0\sqrt{Y_i-\sin\alpha_0}-\sin\alpha_0\sqrt{\tilde{E}Fr-Y_i}.$$

By taking the square, we deduce that

$$\frac{Fr}{2}=\left(\cos\alpha_0\sqrt{Y_i-\sin\alpha_0}-\sin\alpha_0\sqrt{\tilde{E}Fr-Y_i}\right)^2,$$

and so

$$\frac{Fr}{2}=\cos^2\alpha_0\left[Y_i-\sin\alpha_0\right]+\sin^2\alpha_0\left[\tilde{E}Fr-Y_i\right]-2\cos\alpha_0\sin\alpha_0\sqrt{Y_i-\sin\alpha_0}\sqrt{\tilde{E}Fr-Y_i}.$$

We get

$$2\cos\alpha_0\sin\alpha_0\sqrt{Y_i-\sin\alpha_0}\sqrt{\tilde{E}Fr-Y_i}=\cos^2\alpha_0\left[Y_i-\sin\alpha_0\right]+\sin^2\alpha_0\left[\tilde{E}Fr-Y_i\right]-\frac{Fr}{2}$$

and so

$$2\cos\alpha_0\sin\alpha_0\sqrt{Y_i-\sin\alpha_0}\sqrt{\tilde{E}Fr-Y_i}=Y_i\left[\cos^2\alpha_0-\sin^2\alpha_0\right]+\sin^2\alpha_0\tilde{E}Fr-\cos^2\alpha_0\sin\alpha_0-\frac{Fr}{2}.$$

Taking the square again, we get

$$\sin^2 2\alpha_0\left[Y_i-\sin\alpha_0\right]\left[\tilde{E}Fr-Y_i\right]=\left\{Y_i\left[\cos^2\alpha_0-\sin^2\alpha_0\right]+\sin^2\alpha_0\tilde{E}Fr-\cos^2\alpha_0\sin\alpha_0-\frac{Fr}{2}\right\}^2.$$

Therefore

$$-Y_i^2\sin^2 2\alpha_0+\sin^2 2\alpha_0\left[\tilde{E}Fr+\sin\alpha_0\right]Y_i-\sin^2 2\alpha_0\sin\alpha_0\tilde{E}Fr=$$

$$Y_i^2\cos^2 2\alpha_0+2Y_i\cos 2\alpha_0\left[\sin^2\alpha_0\tilde{E}Fr-\cos^2\alpha_0\sin\alpha_0-\frac{Fr}{2}\right]+\left[\sin^2\alpha_0\tilde{E}Fr-\cos^2\alpha_0\sin\alpha_0-\frac{Fr}{2}\right]^2.$$

This implies

$$Y_i^2+Y_i\left[2\cos 2\alpha_0\sin^2\alpha_0\tilde{E}Fr-2\cos 2\alpha_0\cos^2\alpha_0\sin\alpha_0-Fr\cos 2\alpha_0-\sin^2 2\alpha_0\tilde{E}Fr-\sin^2 2\alpha_0\sin\alpha_0\right]$$

$$+\left[\sin^2\alpha_0\tilde{E}Fr-\cos^2\alpha_0\sin\alpha_0-\frac{Fr}{2}\right]^2+\sin^2 2\alpha_0\sin\alpha_0\tilde{E}Fr=0.$$

Using basic trigonometry, we can simplify the expression

$$2\cos 2\alpha_0\sin^2\alpha_0\tilde{E}Fr-2\cos 2\alpha_0\cos^2\alpha_0\sin\alpha_0-Fr\cos 2\alpha_0-\sin^2 2\alpha_0\tilde{E}Fr-\sin^2 2\alpha_0\sin\alpha_0$$

into the expression

$$-2\sin^2\alpha_0\tilde{E}Fr-2\cos^2\alpha_0\sin\alpha_0-Fr\left(\cos^2\alpha_0-\sin^2\alpha_0\right).$$

This gives

$$\begin{aligned}Y_i^2\;&+\;Y_i\left[-2\sin^2\alpha_0\tilde{E}Fr-2\cos^2\alpha_0\sin\alpha_0-Fr\left(\cos^2\alpha_0-\sin^2\alpha_0\right)\right]\\&+\left[\sin^2\alpha_0\tilde{E}Fr-\cos^2\alpha_0\sin\alpha_0-\frac{Fr}{2}\right]^2+4\sin^3\alpha_0\cos^2\alpha_0\tilde{E}Fr=0.\end{aligned}$$

This is a second order polynomial equation in Y_i. The discriminant of this equation is given by

$$\Delta=b^2-4ac=$$

$$4\left\{\sin^4\alpha_0\tilde{E}_s^2Fr^2+\cos^4\alpha_0\sin^2\alpha_0+\frac{Fr^2}{4}\cos^2(2\alpha)+2\tilde{E}Fr\sin^3\alpha_0\cos^2\alpha_0+\sin^2\alpha_0\tilde{E}Fr^2\cos(2\alpha_0)+\cos^2\alpha_0\sin\alpha_0\cos(2\alpha_0)Fr\right\}$$

$$-4\left\{\sin^4\alpha_0\tilde{E}_s^2Fr^2+\cos^4\alpha_0\sin^2\alpha_0+\frac{Fr^2}{4}-2\tilde{E}Fr\sin^3\alpha_0\cos^2\alpha_0-\sin^2\alpha_0\tilde{E}Fr^2+\cos^2\alpha_0\sin\alpha_0Fr\right\}-16\tilde{E}Fr\sin^3\alpha_0\cos^2\alpha_0.$$

Simplifying, we get

$$\begin{aligned}\Delta\;&=\;Fr^2\cos 2\alpha_0+4\tilde{E}Fr^2\sin^2\alpha_0\cos(2\alpha_0)+4\cos^2\alpha_0\sin\alpha_0\cos(2\alpha_0)Fr-Fr^2-4Fr\cos^2\alpha_0\sin\alpha_0+4\sin^2\alpha_0\tilde{E}Fr^2\\&=-Fr^2\left(1-\cos^2(2\alpha_0)\right)+4\sin^2\alpha_0\tilde{E}Fr^2\left[1+\cos(2\alpha_0)\right]+4\cos^2\alpha_0\sin\alpha_0\cos(2\alpha_0)Fr-4Fr\cos^2\alpha_0\sin\alpha_0\\&-\;Fr^2\sin^2(2\alpha_0)+4\sin^2\alpha_0\tilde{E}Fr^2*2\cos^2\alpha_0+4\cos^2\alpha_0\sin\alpha_0Fr\left[-1+\cos(2\alpha_0)\right]\\&-\;Fr^2\sin^2(2\alpha_0)+8\sin^2\alpha_0\tilde{E}Fr^2\cos^2\alpha_0-4\cos^2\alpha_0\sin\alpha_0Fr*2\sin^2\alpha_0=Fr\sin^2(2\alpha_0)\left\{-Fr+2\tilde{E}Fr-2\sin\alpha_0\right\},\end{aligned}$$

which implies that

$$\Delta=Fr\sin^2(2\alpha_0)\left\{-Fr+2\tilde{E}Fr-2\sin\alpha_0\right\}.$$

Therefore, the apex height solution is given by

$$Y_i=\frac{1}{2}\left\{\left[2\sin^2\alpha_0\tilde{E}Fr+2\cos^2\alpha_0\sin\alpha_0+Fr\left(\cos^2\alpha_0-\sin^2\alpha_0\right)\right]\pm\sqrt{Fr\sin^2(2\alpha_0)\left\{-Fr+2\tilde{E}Fr-2\sin\alpha_0\right\}}\right\},$$

which, since $0<\alpha_0<\frac{\pi}{2}$, becomes

$$=\left[\sin^2\alpha_0\tilde{E}Fr+\cos^2\alpha_0\sin\alpha_0+\frac{Fr}{2}\left(\cos^2\alpha_0-\sin^2\alpha_0\right)\right]\pm\sqrt{Fr}\sin\alpha_0\cos\alpha_0\sqrt{\left\{-Fr+2\tilde{E}Fr-2\sin\alpha_0\right\}}.$$

This formula can be then simplified to:

$$Y_i=\sin\alpha_0+\frac{1}{2}\left(\sqrt{Fr}\cos\alpha_0\pm\sin\alpha_0\sqrt{\left\{-Fr+2\tilde{E}Fr-2\sin\alpha_0\right\}}\right)^2.$$

With similar computations, we obtain

$$Y_i=\tilde{E}Fr-\frac{1}{2}\left(\sqrt{Fr}\sin\alpha_0\pm\cos\alpha_0\sqrt{\left\{-Fr+2\tilde{E}Fr-2\sin\alpha_0\right\}}\right)^2.$$

By plugging these solutions, inside

$$-\sqrt{\frac{Fr}{2}}=\cos\alpha_0\sqrt{Y_i-\sin\alpha_0}-\sin\alpha_0\sqrt{\tilde{E}Fr-Y_i},$$

we get that the only possible solutions are

$$\begin{aligned}Y_i\;&=\;\sin\alpha_0+\frac{1}{2}\left(\sqrt{Fr}\cos\alpha_0-\sin\alpha_0\sqrt{\left\{-Fr+2\tilde{E}Fr-2\sin\alpha_0\right\}}\right)^2\\&=\;\tilde{E}Fr-\frac{1}{2}\left(\sqrt{Fr}\sin\alpha_0+\cos\alpha_0\sqrt{\left\{-Fr+2\tilde{E}Fr-2\sin\alpha_0\right\}}\right)^2.\end{aligned}$$

A.4. Proof of the stability properties of the apex return map

This section is dedicating to the deduction of formula (9). Expanding $F(Y_i)$, we get

$$F(Y_i)=\cos^2(\Delta\phi-2\alpha_0)\left[Y_i-\sin\alpha_0\right]+\sin^2(\Delta\phi-2\alpha_0)\left[\tilde{E}Fr-Y_i\right]+\sin(2[\Delta\phi-2\alpha_0])\sqrt{Y_i-\sin\alpha_0}\sqrt{\tilde{E}Fr-Y_i}+\sin(\alpha_0-\Delta\phi).$$

For the stability of the fixed points of the apex return map, we need to satisfy the following condition on the map F:

$$\left|\frac{\partial F}{\partial Y_i}\right|_{Y_{i+1}=Y_i}<1.$$

Given that at the symmetric fixed point $Y_{i+1} = Y_i$, we have $\Delta\phi = 2\alpha_0 - \pi$, we obtain

$$\frac{\partial F}{\partial Y_i} = -2\cos(\Delta\phi - 2\alpha_0)\sin(\Delta\phi - 2\alpha_0)\left[Y_i - \sin\alpha_0\right]\partial_{Y_i}\Delta\phi + \cos^2(\Delta\phi - 2\alpha_0)$$

$$+2\cos(\Delta\phi - 2\alpha_0)\sin(\Delta\phi - 2\alpha_0)\left[\tilde{E} - Y_i\right]\partial_{Y_i}\Delta\phi - \sin^2(\Delta\phi - 2\alpha_0)$$

$$+2\cos(2[\Delta\phi - 2\alpha_0])\partial_{Y_i}\Delta\phi\sqrt{Y_i - \sin\alpha_0}\sqrt{\tilde{E}Fr - Y_i} + \sin(2[\Delta\phi - 2\alpha_0])\frac{\partial}{\partial Y_i}\left[\sqrt{Y_i - \sin\alpha_0}\sqrt{\tilde{E}Fr - Y_i}\right] - \cos(\alpha_0 - \Delta\phi)\partial_{Y_i}\Delta\phi.$$

Therefore

$$\frac{\partial F}{\partial Y_i}\Big|_{Y_{i+1}=Y_i} = \frac{\partial F}{\partial Y_i}\Big|_{\Delta\phi=2\alpha_0-\pi} = 1 + \left[\cos(\alpha_0) + 2\sqrt{Y_i - \sin\alpha_0}\sqrt{\tilde{E}Fr - Y_i}\right]\partial_{Y_i}\Delta\phi.$$

Recall that

$$\frac{\partial}{\partial y_i} = \frac{\partial Y_i}{\partial y_i}\frac{\partial}{\partial Y_i} = \frac{1}{l_0}\frac{\partial}{\partial Y_i}$$

and so that

$$\frac{\partial y^*}{\partial y_i} = \frac{1}{l_0}\frac{\partial[l_0 Y^*]}{\partial Y_i} = \frac{\partial Y^*}{\partial Y_i}.$$

Therefore

$$\frac{\partial Y^*}{\partial Y_i} = 1 + \left[\cos(\alpha_0) + 2\sqrt{Y_i - \sin\alpha_0}\sqrt{\tilde{E}Fr - Y_i}\right]\partial_{Y_i}\Delta\phi.$$

Remember that from the expression for the apex to touch-down map (formula (24) in Geyer et al. (2005)), we have

$$\omega = \sqrt{\frac{2g}{l_0}}\left(\cos\alpha_0\sqrt{Y_i - \sin\alpha_0} - \sin\alpha_0\sqrt{\tilde{E}Fr - Y_i}\right)$$

and therefore

$$\frac{\partial\omega}{\partial Y_i} = \sqrt{\frac{g}{2l_0}}\left(\cos\alpha_0\frac{1}{\sqrt{Y_i - \sin\alpha_0}} + \sin\alpha_0\frac{1}{\sqrt{\tilde{E}Fr - Y_i}}\right).$$

The stability of the apex return map depends then on the variation of the angle swept during stance with respect to the apex height or, equivalently, with respect to the normalized apex height:

$$\partial_i\Delta\phi^* := \frac{\partial}{\partial_{Y_i}}\Big|_{\Delta\phi=2\alpha_0-\phi}\Delta\phi.$$

We have

$$\partial_i\Delta\phi = 2\partial_i\left[\frac{\omega}{\hat{\omega}_0}\left\{\arccos\left(\frac{a}{b}\right)\right\}\right] = 2\partial_i\left[\frac{\omega}{\hat{\omega}_0}\right]\left\{\arccos\left(\frac{a}{b}\right)\right\} + 2\frac{\omega}{\hat{\omega}_0}\partial_i\left[\left\{\arccos\left(\frac{a}{b}\right)\right\}\right].$$

Note that, by the chain rule, we have:

$$\partial_i\left[\frac{\omega}{\hat{\omega}_0}\right] = \frac{\partial\omega}{\partial Y_i}\frac{\partial}{\partial\omega}\left[\frac{\omega}{\hat{\omega}_0}\right] = \partial_i\omega\frac{\partial}{\partial\omega}\frac{\omega}{\sqrt{3\omega^2 + \omega_0^2}} = \partial_i\omega\frac{\sqrt{3\omega^2 + \omega_0^2} - \frac{3*2\omega}{2\sqrt{3\omega^2+\omega_0^2}}}{3\omega^2 + \omega_0^2} = \frac{3\omega^2 + \omega_0^2 - 3\omega^2}{(3\omega^2 + \omega_0^2)^{3/2}}\partial_i\omega = \frac{\omega_0^2}{(3\omega^2 + \omega_0^2)^{3/2}}\partial_i\omega.$$

By the definition of the derivative of arccos and by the chain rule, this becomes:

$$\partial_i\left[\left\{\arccos\left(\frac{a}{b}\right)\right\}\right] = \frac{\partial\omega}{\partial Y_i}\frac{\partial}{\partial\omega}\left[\left\{\arccos\left(\frac{a}{b}\right)\right\}\right] = \frac{\partial\omega}{\partial Y_i}\frac{\partial}{\partial\omega}\left[\arccos\left(\frac{\omega^2 - (g\sin\alpha_0)/l_0}{\sqrt{(\omega^2 - (g\sin\alpha_0)/l_0)^2 + (3\omega^2 + \omega_0^2)\dot{r}_0^2/l_0^2}}\right)\right]$$

$$= -\frac{\partial\omega}{\partial Y_i}\frac{1}{\sqrt{1 - \left(\frac{\omega^2 - (g\sin\alpha_0)/l_0}{\sqrt{(\omega^2 - (g\sin\alpha_0)/l_0)^2 + (3\omega^2 + \omega_0^2)\dot{r}_0^2/l_0^2}}\right)^2}}\frac{\partial}{\partial\omega}\left(\frac{\omega^2 - (g\sin\alpha_0)/l_0}{\sqrt{(\omega^2 - (g\sin\alpha_0)/l_0)^2 + (3\omega^2 + \omega_0^2)\dot{r}_0^2/l_0^2}}\right)$$

$$= -\frac{1}{\sqrt{\frac{(3\omega^2+\omega_0^2)\dot{r}_0^2/l_0^2}{(\omega^2 - (g\sin\alpha_0)/l_0)^2 + (3\omega^2+\omega_0^2)\dot{r}_0^2/l_0^2}}}\frac{\partial\omega}{\partial Y_i}\frac{\partial}{\partial\omega}\left(\frac{\omega^2 - (g\sin\alpha_0)/l_0}{\sqrt{(\omega^2 - (g\sin\alpha_0)/l_0)^2 + (3\omega^2 + \omega_0^2)\dot{r}_0^2/l_0^2}}\right)$$

$$= -\frac{\sqrt{(\omega^2 - (g\sin\alpha_0)/l_0)^2 + (3\omega^2 + \omega_0^2)\dot{r}_0^2/l_0^2}}{\sqrt{(3\omega^2 + \omega_0^2)\dot{r}_0^2/l_0^2}}\frac{\partial\omega}{\partial Y_i}\frac{\partial}{\partial\omega}\left(\frac{\omega^2 - (g\sin\alpha_0)/l_0}{\sqrt{(\omega^2 - (g\sin\alpha_0)/l_0)^2 + (3\omega^2 + \omega_0^2)\dot{r}_0^2/l_0^2}}\right)$$

By expanding the partial derivative with respect to $\frac{\partial}{\partial\omega}$ and, again, by the chain rule, we have:

$$= -\frac{\sqrt{(\omega^2-(g\sin\alpha_0)/l_0)^2+(3\omega^2+\omega_0^2)\dot{r}_0^2/l_0^2}}{\sqrt{(3\omega^2+\omega_0^2)\dot{r}_0^2/l_0^2}}\frac{\partial\omega}{\partial Y_i}$$
$$\times \frac{2\omega\sqrt{(\omega^2-(g\sin\alpha_0)/l_0)^2+(3\omega^2+\omega_0^2)\dot{r}_0^2/l_0^2}-\frac{(\omega^2-(g\sin\alpha_0)/l_0)*\left\{2(\omega^2-(g\sin\alpha_0)/l_0)*2\omega+6\omega\dot{r}_0^2/l_0^2\right\}}{2\sqrt{(\omega^2-(g\sin\alpha_0)/l_0)^2+(3\omega^2+\omega_0^2)\dot{r}_0^2/l_0^2}}}{(\omega^2-(g\sin\alpha_0)/l_0)^2+(3\omega^2+\omega_0^2)\dot{r}_0^2/l_0^2}$$

Simplifying even further, we get:

$$= -\frac{1}{\sqrt{(3\omega^2+\omega_0^2)\dot{r}_0^2/l_0^2}}\frac{\partial\omega}{\partial Y_i}$$
$$\times \frac{2\omega\left((\omega^2-(g\sin\alpha_0)/l_0)^2+(3\omega^2+\omega_0^2)\dot{r}_0^2/l_0^2\right)-\left((\omega^2-(g\sin\alpha_0)/l_0)*\left\{2(\omega^2-(g\sin\alpha_0)/l_0)\omega+3\omega\dot{r}_0^2/l_0^2\right)\right\}}{(\omega^2-(g\sin\alpha_0)/l_0)^2+(3\omega^2+\omega_0^2)\dot{r}_0^2/l_0^2}$$
$$= -\frac{2\omega(3\omega^2+\omega_0^2)\dot{r}_0^2/l_0^2-3\omega(\omega^2-(g\sin\alpha_0)/l_0)\dot{r}_0^2/l_0^2}{\left[(\omega^2-(g\sin\alpha_0)/l_0)^2+(3\omega^2+\omega_0^2)\dot{r}_0^2/l_0^2\right]\sqrt{(3\omega^2+\omega_0^2)\dot{r}_0^2/l_0^2}}\frac{\partial\omega}{\partial Y_i}$$

Putting all of these computations together, we get:

$$\partial_i\ \Delta\phi = 2\partial_i\left[\frac{\omega}{\hat{\omega}_0}\right]\left\{\arccos\left(\frac{a}{b}\right)\right\}+2\frac{\omega}{\hat{\omega}_0}\partial_i\left[\left\{\arccos\left(\frac{a}{b}\right)\right\}\right]$$
$$= 2\frac{\omega_0^2}{(3\omega^2+\omega_0^2)^{3/2}}\frac{\partial\omega}{\partial Y_i}\left\{\arccos\left(\frac{a}{b}\right)\right\}-2\frac{\omega}{\hat{\omega}_0}\frac{[2(3\omega^2+\omega_0^2)-3(\omega^2-(g\sin\alpha_0)/l_0)]\omega\dot{r}_0^2/l_0^2}{\left[(\omega^2-(g\sin\alpha_0)/l_0)^2+(3\omega^2+\omega_0^2)\dot{r}_0^2/l_0^2\right]\sqrt{(3\omega^2+\omega_0^2)\dot{r}_0^2/l_0^2}}\frac{\partial\omega}{\partial Y_i}$$
$$= \frac{2}{\hat{\omega}_0^3}\left\{\omega_0^2\left\{\arccos\left(\frac{\omega^2-(g\sin\alpha_0)/l_0}{\sqrt{(\omega^2-(g\sin\alpha_0)/l_0)^2+\hat{\omega}_0^2\dot{r}_0^2/l_0^2}}\right)\right\}-\frac{[2\hat{\omega}_0^2-3(\omega^2-(g\sin\alpha_0)/l_0)]\omega^2\hat{\omega}_0\dot{r}_0^2/l_0^2}{\left[(\omega^2-(g\sin\alpha_0)/l_0)^2+\hat{\omega}_0^2\dot{r}_0^2/l_0^2\right]\sqrt{\dot{r}_0^2/l_0^2}}\right\}\frac{\partial\omega}{\partial Y_i}.$$

Hence

$$\partial_i\ \Delta\phi = \frac{2}{\hat{\omega}_0^3}\sqrt{\frac{g}{2l_0}}\left\{\omega_0^2\left\{\arccos\left(\frac{\omega^2-(g\sin\alpha_0)/l_0}{\sqrt{(\omega^2-(g\sin\alpha_0)/l_0)^2+\hat{\omega}_0^2\dot{r}_0^2/l_0^2}}\right)\right\}-\frac{[2\hat{\omega}_0^2-3(\omega^2-(g\sin\alpha_0)/l_0)]\omega^2\hat{\omega}_0\sqrt{\dot{r}_0^2/l_0^2}}{(\omega^2-(g\sin\alpha_0)/l_0)^2+\hat{\omega}_0^2\dot{r}_0^2/l_0^2}\right\}$$
$$\times\left(\cos\alpha_0\frac{1}{\sqrt{Y_i-\sin\alpha_0}}+\sin\alpha_0\frac{1}{\sqrt{\tilde{E}Fr-Y_i}}\right),$$

with

$$Y_i = \sin\alpha_0+\frac{1}{2}\left(\sqrt{Fr}\cos\alpha_0-\sin\alpha_0\sqrt{\left\{-Fr+2\tilde{E}Fr-2\sin\alpha_0\right\}}\right)^2$$
$$= \tilde{E}Fr-\frac{1}{2}\left(\sqrt{Fr}\sin\alpha_0+\cos\alpha_0\sqrt{\left\{-Fr+2\tilde{E}Fr+2\sin\alpha_0\right\}}\right)^2.$$

We have

$$\partial_i\ \Delta\phi = \frac{\sqrt{2}\tilde{k}}{\sqrt{Fr}(\tilde{k}+3)^{3/2}}\left\{\left\{\arccos\left(\frac{\omega^2(1-\sin\alpha_0/Fr)}{\sqrt{(\omega^2(1-\sin\alpha_0/Fr))^2+(\tilde{k}+3)\omega^2\omega^2/Fr[2\tilde{E}Fr-Fr-2\sin\alpha_0]}}\right)\right\}\right\}$$
$$\times\left(\cos\alpha_0\frac{1}{\sqrt{Y_i-\sin\alpha_0}}+\sin\alpha_0\frac{1}{\sqrt{\tilde{E}Fr-Y_i}}\right)$$
$$-\left\{\frac{\sqrt{2}}{\sqrt{Fr}\omega^2(\tilde{k}+3)^{3/2}}\frac{[2[\omega^2(\tilde{k}+3)]-3\omega^2(1-\sin\alpha_0/Fr)]\omega^2|\omega|\sqrt{\tilde{k}+3}\sqrt{\omega^2/Fr[2\tilde{E}Fr-Fr-2\sin\alpha_0]}}{(\omega^2(1-\sin\alpha_0/Fr))^2+(\tilde{k}+3)\omega^2\omega^2/Fr[2\tilde{E}Fr-Fr-2\sin\alpha_0]}\right\}$$
$$\times\left(\cos\alpha_0\frac{1}{\sqrt{Y_i-\sin\alpha_0}}+\sin\alpha_0\frac{1}{\sqrt{\tilde{E}Fr-Y_i}}\right).$$

Simplifying further, we get:

$$\partial_i\ \Delta\phi = \frac{\sqrt{2}\tilde{k}}{\sqrt{Fr}(\tilde{k}+3)^{3/2}}\left\{\arccos\left(\frac{(1-\sin\alpha/_0Fr)}{\sqrt{(1-\sin\alpha_0/Fr)^2+(\tilde{k}+3)/Fr[2\tilde{E}Fr-Fr-2\sin\alpha_0]}}\right)\right\}$$

$$\times \left(\cos\alpha_0 \frac{1}{\sqrt{Y_i - \sin\alpha_0}} + \sin\alpha_0 \frac{1}{\sqrt{\tilde{E}Fr - Y_i}} \right)$$

$$- \left\{ \frac{\sqrt{2}}{\sqrt{Fr}(\tilde{k}+3)^{3/2}} \frac{[2(\tilde{k}+3) - 3(1-\sin\alpha_0/Fr)]\sqrt{\tilde{k}+3}\sqrt{1/Fr[2\tilde{E}Fr - Fr - 2\sin\alpha_0]}}{(1-\sin\alpha_0/Fr)^2 + (\tilde{k}+3)1/Fr[2\tilde{E}Fr - Fr - 2\sin\alpha_0]} \right\}$$

$$\times \left(\cos\alpha_0 \frac{1}{\sqrt{Y_i - \sin\alpha_0}} + \sin\alpha_0 \frac{1}{\sqrt{\tilde{E}Fr - Y_i}} \right)$$

and so

$$\partial_i \ \Delta\phi = \frac{\sqrt{2}\tilde{k}}{\sqrt{Fr}(\tilde{k}+3)^{3/2}} \left\{ \arccos\left(\frac{(1-\sin\alpha_0/Fr)}{\sqrt{(1-\sin\alpha_0/Fr)^2 + (\tilde{k}+3)[2\tilde{E} - 1 - 2\sin\alpha_0/Fr]}} \right) \right\}$$

$$\times \left(\cos\alpha_0 \frac{1}{\sqrt{Y_i - \sin\alpha_0}} + \sin\alpha_0 \frac{1}{\sqrt{\tilde{E}Fr - Y_i}} \right)$$

$$- \left\{ \frac{\sqrt{2}}{\sqrt{Fr}(\tilde{k}+3)^{3/2}} \frac{[2(\tilde{k}+3) - 3(1-\sin\alpha_0/Fr)]\sqrt{\tilde{k}+3}\sqrt{2\tilde{E} - 1 - 2\sin\alpha_0/Fr}}{(1-\sin\alpha/Fr)^2 + (\tilde{k}+3)[2\tilde{E} - 1 - 2\sin\alpha_0/Fr]} \right\}$$

$$\times \left(\cos\alpha_0 \frac{1}{\sqrt{Y_i - \sin\alpha_0}} + \sin\alpha_0 \frac{1}{\sqrt{\tilde{E}Fr - Y_i}} \right).$$

Inserting this last formula in

$$\frac{\partial Y_{i+1}}{\partial Y_i}|_{Y_{i+1}=Y_i=Y^*} = 1 + \left[\cos(\alpha_0) + 2\sqrt{Y_i - \sin\alpha_0}\sqrt{\tilde{E}Fr - Y_i} \right] \partial_{Y_i} \Delta\phi,$$

we obtain an explicit expression for $\frac{\partial Y_{i+1}}{\partial Y_i}|_{Y_{i+1}=Y_i=Y^*}$ for $\Delta\phi = 2\alpha_0 - \pi$ and so an explicit expression to verify the stability condition

$$\left| \frac{\partial F}{\partial Y_i} \right|_{Y_{i+1}=Y_i} < 1.$$

A.5. Error analysis

In this subsection, we perform an error analysis of our approximation to the apex return map. An interesting consequence of this is the quantification of the link between the hypotheses of small compression, small angle swept during stance, and error produced by our approximation of the apex return map. We also include heat maps describing the accuracy of our approximation.

A.5.1. Rigorous bounds

Consider again the normalized apex return map:

$$F(Y_i) = \cos^2(\Delta\phi - 2\alpha_0)\left[Y_i - \sin\alpha_0\right] + \sin^2(\Delta\phi - 2\alpha_0)\left[\tilde{E}Fr - Y_i\right] + \sin(2[\Delta\phi - 2\alpha_0])\sqrt{Y_i - \sin\alpha_0}\sqrt{\tilde{E}Fr - Y_i} + \sin(\alpha_0 - \Delta\phi).$$

We use a distinct notation for the apex return map, that for this paragraph we call F_δ, computed using our approximation and define $\Delta\psi := \Delta\phi + \delta$, with δ the error made in the angle swept during stance with our approximation. We have

$$F_\delta(Y_i) = \cos^2(\Delta\psi - 2\alpha_0)\left[Y_i - \sin\alpha_0\right] + \sin^2(\Delta\psi - 2\alpha_0)\left[\tilde{E}Fr - Y_i\right] + \sin(2[\Delta\psi - 2\alpha_0])\sqrt{Y_i - \sin\alpha_0}\sqrt{\tilde{E}Fr - Y_i} + \sin(\alpha_0 - \Delta\psi).$$

We decompose $F_\delta(Y_i) - F(Y_i) := I + II$, with

$$I := \cos^2(\Delta\psi - 2\alpha_0)\left[Y_i - \sin\alpha_0\right] + \sin^2(\Delta\psi - 2\alpha_0)\left[\tilde{E}Fr - Y_i\right] + \sin(2[\Delta\psi - 2\alpha_0])\sqrt{Y_i - \sin\alpha_0}\sqrt{\tilde{E}Fr - Y_i}$$

$$- \left\{ \cos^2(\Delta\phi - 2\alpha_0)\left[Y_i - \sin\alpha_0\right] + \sin^2(\Delta\phi - 2\alpha_0)\left[\tilde{E}Fr - Y_i\right] + \sin(2[\Delta\phi - 2\alpha_0])\sqrt{Y_i - \sin\alpha_0}\sqrt{\tilde{E}Fr - Y_i} \right\}$$

and

$$II := \sin(\alpha_0 - \Delta\psi) - \sin(\alpha_0 - \Delta\phi).$$

We start from II. Expanding around $\alpha_0 - \Delta\phi$, we get

$$II = \sin(\alpha_0 - \Delta\phi)\cos(-\delta) - \cos(\alpha_0 - \Delta\phi)\sin(-\delta) - \sin(\alpha_0 - \Delta\phi) = \sin(\alpha_0 - \Delta\phi)(\cos(\delta) - 1) - \cos(\alpha_0 - \Delta\phi)\sin(-\delta).$$

Therefore, we obtain

$$|II| \leq |1 - \cos(\delta)||\sin(\alpha_0 - \Delta\phi)| + |\sin(\delta)||\cos(\alpha_0 - \Delta\phi)| \leq \frac{\delta^2}{2} + \delta,$$

which implies

$$\|II\|_{L^\infty} \leq C\delta.$$

We continue with I. We decompose this term further as $I := A + B + C$, with

$$A := \left\{\cos^2(\Delta\psi - 2\alpha_0) - \cos^2(\Delta\phi - 2\alpha_0)\right\}\left[Y_i - \sin\alpha_0\right],$$

$$B := \left\{\sin^2(\Delta\psi - 2\alpha_0) - \sin^2(\Delta\phi - 2\alpha_0)\right\}\left[\tilde{E}Fr - Y_i\right],$$

and

$$C := \left\{\sin(2[\Delta\psi - 2\alpha_0]) - \sin(2[\Delta\phi - 2\alpha_0])\right\}\sqrt{Y_i - \sin\alpha_0}\sqrt{\tilde{E}Fr - Y_i}.$$

Expanding A around $\Delta\psi - 2\alpha_0$, we get

$$A = \left\{[\cos(\Delta\phi - 2\alpha_0)\cos(\delta) + \sin(\Delta\phi - 2\alpha_0)\sin(\delta)]^2 - \cos^2(\Delta\phi - 2\alpha_0)\right\}\left[Y_i - \sin\alpha_0\right],$$

while expanding the squares, we get

$$A = \left\{[\cos^2(\Delta\phi - 2\alpha_0)(\cos^2(\delta) - 1) + \sin^2(\Delta\phi - 2\alpha_0)\sin^2(\delta) + 2\sin(\Delta\phi - 2\alpha_0)\cos(\Delta\phi - 2\alpha_0)\sin(\delta)\cos(\delta)]\right\}\left[Y_i - \sin\alpha_0\right].$$

Bounding A again in L^∞ norm, we have:

$$\|A\|_{L^\infty} \leq \delta^2 + \delta^2 + \delta \leq C\delta.$$

Similar computations can be developed for term B:

$$B := \left\{[\sin(\Delta\phi - 2\alpha_0)\cos(\delta) + \cos(\Delta\phi - 2\alpha_0)\sin(\delta)]^2 - \sin^2(\Delta\phi - 2\alpha_0)\right\}\left[\tilde{E}Fr - Y_i\right] =$$

$$\left\{[\sin^2(\Delta\psi - 2\alpha_0)(\cos^2(\delta) - 1) + \cos^2(\Delta\psi - 2\alpha_0)\sin^2(\delta) + 2\sin(\Delta\psi - 2\alpha_0)\cos(\delta)\cos(\Delta\psi - 2\alpha_0)\sin(\delta)]\right\}\left[\tilde{E}Fr - Y_i\right].$$

Bounding B in L^∞ norm, we have:

$$\|B\|_{L^\infty} \leq \left|\tilde{E}Fr - Y_i\right|(\delta^2 + \delta^2 + \delta) \leq C(Fr, \tilde{E})(\delta^2 + \delta^2 + \delta) \leq C(Fr, \tilde{E})\delta.$$

Analogously for term C, we obtain

$$C := \left\{\sin(2[\Delta\phi - 2\alpha_0] + 2\delta) - \sin(2[\Delta\phi - 2\alpha_0])\right\}\sqrt{Y_i - \sin\alpha_0}\sqrt{\tilde{E}Fr - Y_i} =$$

$$\left\{\sin(2[\Delta\phi - 2\alpha_0])\cos(2\delta) + \cos(2[\Delta\phi - 2\alpha_0])\sin(2\delta) - \sin(2[\Delta\phi - 2\alpha_0])\right\}\sqrt{Y_i - \sin\alpha_0}\sqrt{\tilde{E}Fr - Y_i} =$$

$$\left\{\sin(2[\Delta\phi - 2\alpha_0])(\cos(2\delta) - 1) + \cos(2[\Delta\phi - 2\alpha_0])\sin(2\delta)\right\}\sqrt{Y_i - \sin\alpha_0}\sqrt{\tilde{E}Fr - Y_i}.$$

Bounding C as well in L^∞ norm, we have:

$$\|C\|_{L^\infty} \leq \left|\sqrt{\tilde{E}Fr - Y_i}\right|\left|\sqrt{Y_i - \sin\alpha_0}\right|(\delta^2 + \delta) \leq C(Fr, \tilde{E})(\delta^2 + +\delta) \leq C(Fr, \tilde{E})\delta.$$

Put all these estimates together, we obtain

$$\|F_\delta(Y_i) - F(Y_i)\|_{L^\infty} \leq C(Fr, \tilde{E})\delta.$$

This series of deductions gives an explicit bound on the error we make in the apex return map in terms of the error we make in the angle swept during stance. This bound can be rephrased as a bound with respect to small compression, arguing in the following way. In normalized variables and denoting with $\dot{\phi}$ the exact angular velocity and by $\dot{\phi}_a$ our approximation, the error in the angular velocity with our assumption of constant angular velocity is given by

$$\dot{\phi}_a - \dot{\phi} = \omega - \omega\frac{1}{(1+\rho)^2} = 2\rho\omega + o(\rho).$$

Using similar computations to those developed in Appendix A.1 and by integrating $\dot{\phi}_a - \dot{\phi}$ from t_{TD} to t_{TO}, we find

$$|\delta| = |\Delta\phi - \Delta\phi_a| = \left|\int_{t_{TD}}^{t_{TO}} \dot{\phi}_a - \dot{\phi}dt\right| \leq \int_{t_{TD}}^{t_{TO}} \left|\dot{\phi}_a - \dot{\phi}\right|dt \leq \int_{t_{TD}}^{t_{TO}} 2\rho\omega dt \leq 2\epsilon\omega(t_{TO} - t_{TD}) \leq 4\epsilon\frac{\omega}{\hat{\omega}_0}\left\{\arccos\left(\frac{a}{b}\right)\right\},$$

in the time interval of the stance phase deduced from the approximate solution and with the compression small, bounded by $\rho \leq \epsilon$. This implies that

$$|\delta| \leq C\epsilon.$$

In conclusion,

$$\|F_\delta(Y_i) - F(Y_i)\|_{L^\infty} \leq C(Fr, \tilde{E})\delta \leq C(Fr, \tilde{E})\epsilon.$$

This gives an explicit quantitative bound on the error we make in the apex return map under our assumptions; in particular the error made is first order with respect to the size of the compression that we assume to be small.

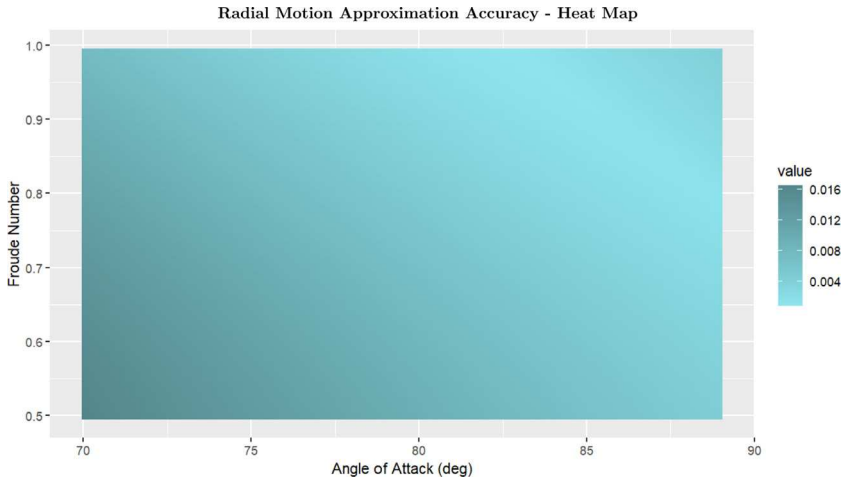

Fig. 9. Radial motion approximation accuracy. Heat map. Rows: Angle of Attack α_0 from 70 deg to 89 deg with increments of 0.1 deg. Columns: Froude Number Fr from 0.5 to 0.995 with increments of 0.01. These plots show the relative error (e_{rel}) of the radial distance of the CoM for our approximation r_a vs. the numerical solution r_n. Here: $m = 80$ kg, $l_0 = 1$ m, $k = 16000$ N/m, and $E = 1200$ J. See Section 3.2.2 for the definition of e_{rel}.

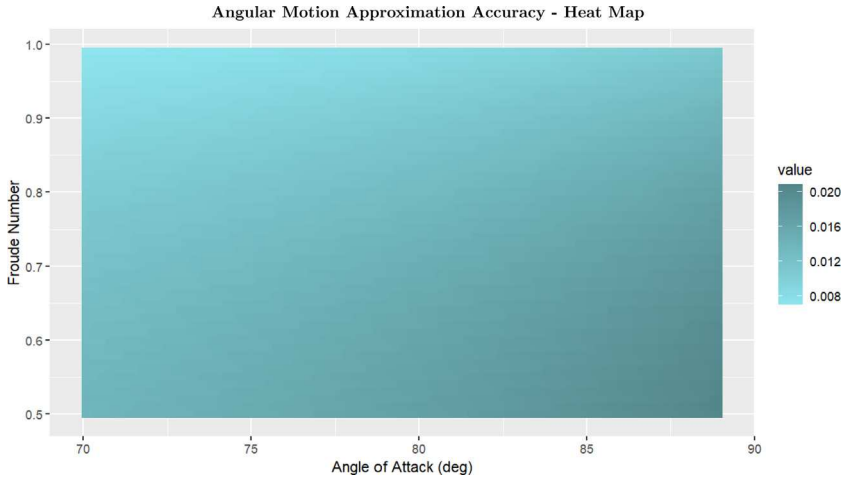

Fig. 10. Angular motion approximation accuracy. Heat map. Rows: Angle of Attack α_0 from 70 deg to 89 deg with increments of 0.1 deg. Columns: Froude Number Fr from 0.5 to 0.995 with increments of 0.01. These plots show the relative error (e_{rel}) of the angular distance of the CoM for our approximation ϕ_a vs. the numerical solution ϕ_n. Here: $m = 80$ kg, $l_0 = 1$ m, $k = 16000$ N/m, and $E = 1200$ J. See Section 3.2.2 for the definition of e_{rel}.

A.5.2. Heat maps

In this appendix, we also include two heat maps describing the error made by our approximation in both the radial (Fig. 9) and angular (Fig. 10) components for an extended range of parameters with an angle of attack α_0 ranging from 70 deg to 89 deg with increments of 1 deg and *Froude number* Fr ranging from 0.5 to 0.995 with increments of 0.05. Note that both radial and angular motions are best approximated by our model at high *Froude numbers*. This is a reflection of the fact that ours is a model of running and running is more difficult at low *Froude numbers*, where walking is preferred (Usherwood, 2005).

A.6. Further data analysis results

In this subsection, we include the full results of the (1) Shapiro–Wilk Normality Test for ϕ and (2) Linear Regression of ϕ vs. t. Both of these results are illustrated for Stride 1 of Subject 1 and for all the three conditions $v = 2.5$ m/s, $v = 3.5$ m/s, and $v = 4.5$ m/s. Furthermore, we include the full results of the (3) Shapiro–Wilk Normality Test for $\Delta\phi$ and (4) Linear Regression of $\Delta\phi$ vs. $\widehat{\Delta\phi}$. Both of these results are illustrated for Subject 1 and for all the three conditions $v = 2.5$ m/s, $v = 3.5$ m/s, and $v = 4.5$ m/s. The calculations have been performed with the first two strides of each trial excluded. This is not a limitation as, in treadmill experiments, it is very likely that the first strides, especially those at high speed, which have a sharp transition from static to moving surface, are needed for the subject to accustom themselves to the experiment. The analysis removing only the first stride from all the three conditions, resulted in a similar outcome, apart from the condition $v = 4.5$ m/s, which gave a p-value < 0.05 with the same tests. In all Shapiro–Wilk Tests, the test is always H_0: "Normal" vs. H_A: "not Normal". In the angular linear fit and angle swept during stance tests, the test performed is a two-sided t-test. In all Shapiro–Wilk Tests, we indicate the test statistic with W. We summarize the results of this section in Tables 2 to 9 and in the Normal QQ plots (Figs. 11 and 12).

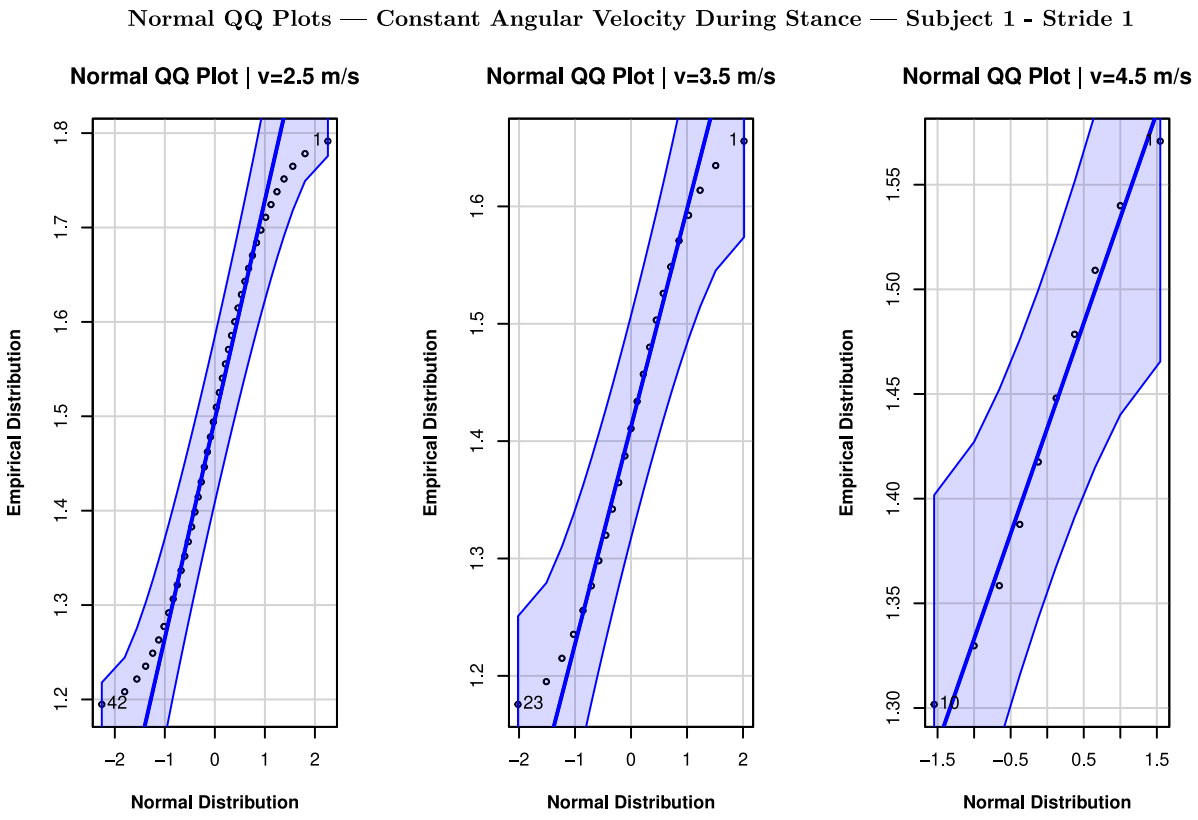

Fig. 11. Normal QQ plots - Constant angular velocity during stance - Subject 1 - Stride 1. The x-axis represents quantiles of the Standard Normal Distribution. The y-axis represents the empirical quantiles of ϕ. Left Plot: At velocity $v = 2.5$ m/s, we have $W = 0.99052$ and p-value $p = 0.8488$. Central Plot: At velocity $v = 3.5$ m/s, we have $W = 0.985$ and p-value $p = 0.4481$. Right Plot: At velocity $v = 4.5$ m/s, we have $W = 0.97285$ and p-value $p = 0.05871$. The tests performed here are Shapiro–Wilk.

Table 2
The linear time component has a significant effect on ϕ at $v = 2.5$ m/s.

$\hat{\omega}$ and $v = 2.5$ m/s - Angular linear fit				
Covariate	Estimate	Std. Error	t-value	p-value
(Intercept)	1.816717	0.001483	1224.9	<**0.0001**
Time	−2.230877	0.009014	−247.5	<**0.0001**

Table 3
The linear time component has a significant effect on ϕ at $v = 3.5$ m/s.

$\hat{\omega}$ and $v = 3.5$ m/s - Angular linear fit				
Covariate	Estimate	Std. Error	t-value	p-value
(Intercept)	1.679230	0.001297	1294.9	<**0.0001**
Time	−3.331498	0.014187	−234.8	<**0.0001**

Table 4
The linear time component has a significant effect on ϕ at $v = 4.5$ m/s.

$\hat{\omega}$ and $v = 4.5$ m/s - Angular linear fit				
Covariate	Estimate	Std. Error	t-value	p-value
(Intercept)	1.599137	0.001002	1596.4	<**0.0001**
Time	−4.499545	0.024215	−185.8	<**0.0001**

Table 5
The null hypothesis of normality of ϕ cannot be rejected at level $\alpha = 0.05$ in any of the three conditions $v = 2.5$ m/s, $v = 3.5$ m/s, and $v = 4.5$ m/s.

Shapiro–Wilk normality test — Angle			
	$v = 2.5$ m/s	$v = 3.5$ m/s	$v = 4.5$ m/s
W statistic	0.94924	0.95339	0.96872
p-value	0.06064	0.3435	0.8788

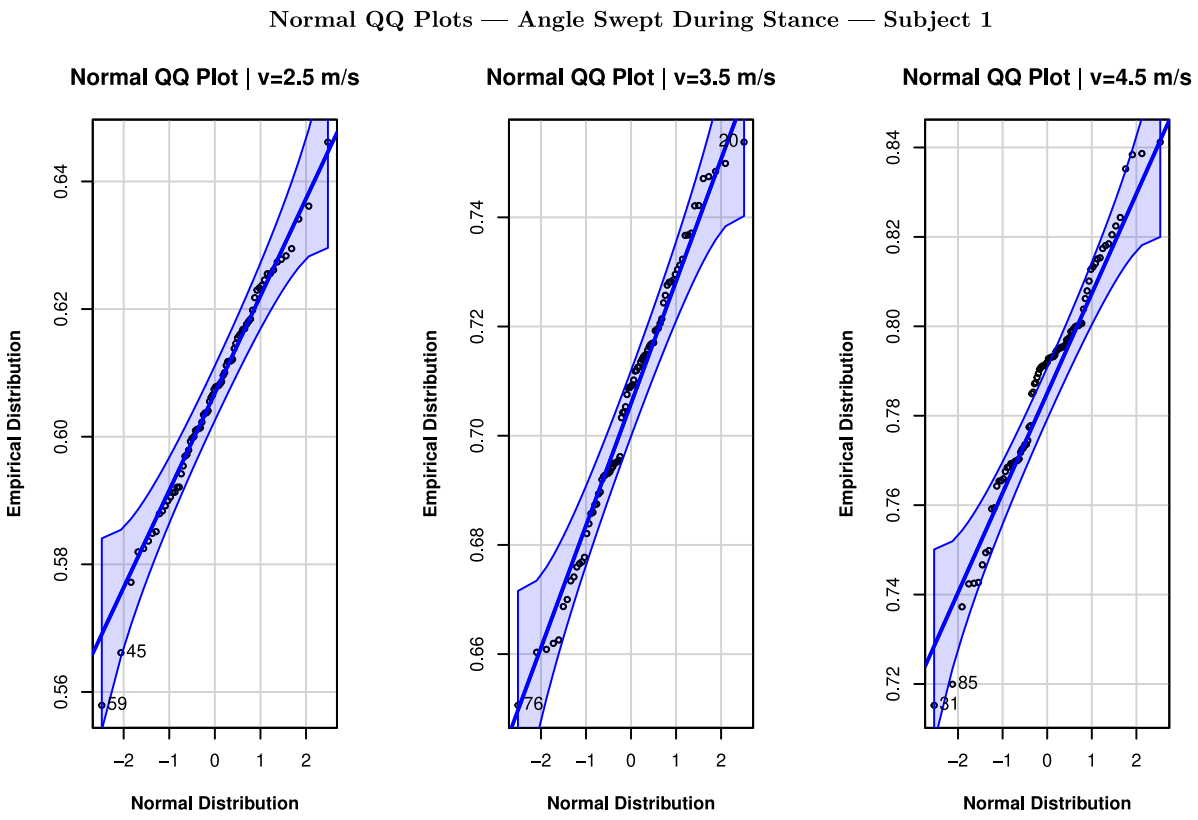

Fig. 12. Normal QQ plots - Angle swept during stance - Subject 1. The x-axis represents quantiles of the Standard Normal Distribution. The y-axis represents the empirical quantiles of $\Delta\phi$. Left Plot: At velocity $v = 2.5$ m/s, we have $W = 0.94924$ and p-value $p = 0.06064$. Central Plot: At velocity $v = 3.5$ m/s, we have $W = 0.95339$ and p-value $p = 0.3435$. Right Plot: At velocity $v = 4.5$ m/s, we have $W = 0.96872$ and p-value $p = 0.8788$. The tests performed here are Shapiro–Wilk.

Table 6
The predicted angle swept during stance $\widehat{\Delta\phi}$ has a significant effect on $\Delta\phi$ at $v = 2.5$ m/s. The calculations have been performed with the first two strides of the trial excluded.

$\Delta\phi$ vs. $\widehat{\Delta\phi}$ and $v = 2.5$ m/s - Angle swept during stance				
Covariate	Estimate	Std. Error	t-value	p-value
(Intercept)	0.016615	0.005009	3.317	**0.00141**
$\widehat{\Delta\phi}$	0.932189	0.007912	117.823	**<0.0001**

Table 7
The predicted angle swept during stance $\widehat{\Delta\phi}$ has a significant effect on $\Delta\phi$ at $v = 3.5$ m/s. The calculations have been performed with the first two strides of the trial excluded.

$\Delta\phi$ vs. $\widehat{\Delta\phi}$ and $v = 3.5$ m/s - Angle swept during stance				
Covariate	Estimate	Std. Error	t-value	p-value
(Intercept)	0.023612	0.003987	5.922	**<0.0001**
$\widehat{\Delta\phi}$	0.920102	0.005371	171.307	**<0.0001**

Table 8
The predicted angle swept during stance $\widehat{\Delta\phi}$ has a significant effect on $\Delta\phi$ at $v = 4.5$ m/s. The calculations have been performed with the first two strides of the trial excluded.

$\Delta\phi$ vs. $\widehat{\Delta\phi}$ and $v = 4.5$ m/s - Angle swept during stance				
Covariate	Estimate	Std. Error	t-value	p-value
(Intercept)	−0.012217	0.002943	−4.151	**<0.0001**
$\widehat{\Delta\phi}$	0.961381	0.003557	270.256	**<0.0001**

A.7. Point by point comparison of our approximation and that in Geyer et al. (2005)

In this subsection, we include Table 10 that gives a point by point comparison between the main features of our model and those of Geyer et al. (2005). Both papers consider the regime of small compression and small angle swept during stance. Among the main differences, our analysis is valid for every Froude number $Fr > 0$, while Geyer et al. (2005) considers a higher order approximation of the angular velocity ϕ.

Table 9
The null hypothesis of normality of $\Delta\phi$ cannot be rejected at level $\alpha = 0.05$ in any of the three conditions $v = 2.5$ m/s, $v = 3.5$ m/s, and $v = 4.5$ m/s.

Shapiro–Wilk normality test — Angle swept during stance			
	$v = 2.5$ m/s	$v = 3.5$ m/s	$v = 4.5$ m/s
W statistic	0.99052	0.985	0.97285
p-value	0.8488	0.4481	0.05871

Table 10
This table compares the main components of our approximation to their counterparts in Geyer et al. (2005).

Comparison with the approximation in Geyer et al. (2005)		
Quantity	Our approximation	The approximation of Geyer et al. (2005)
Froude number	$Fr > 0$	$Fr = 1$
Angular velocity	$\dot{\phi} = \omega$	$\dot{\phi} = \omega(1 - 2\rho)$
Radial position	$r(t) = l_0\left(1 + a + b\sin\hat{\omega}_0 t\right)$	$r(t) = l_0\left(1 + a + b\sin\hat{\omega}_0 t\right)$
a	$\frac{\omega^2 - (g\sin\alpha_0)/l_0}{\omega_0^2 + 3\omega^2}$	$\frac{\omega^2 - g/l_0}{\omega_0^2 + 3\omega^2}$
b	$\frac{\sqrt{(\omega^2 - (g\sin\alpha_0)/l)^2 + (\omega_0^2 + 3\omega^2)(\epsilon - \omega^2 - 2(g\sin\alpha_0)/l_0)}}{\omega_0^2 + \omega^2}$	$\frac{\sqrt{(\omega^2 - g/l)^2 + (\omega_0^2 + 3\omega^2)(\epsilon - \omega^2 - 2g/l_0)}}{\omega_0^2 + \omega^2}$
$\hat{\omega}$	$\hat{\omega}_0 := \sqrt{\omega_0^2 + 3\omega^2}$	$\hat{\omega}_0 := \sqrt{\omega_0^2 + 3\omega^2}$
ω_0	$\sqrt{k/m}$	$\sqrt{k/m}$
Potential energy	$mgr\sin(\alpha_0)$	mgr
Kinetic energy	$\frac{m}{2}\left(\dot{r}^2 + r^2\omega^2\right)$	$\frac{m}{2}\left(\dot{r}^2 + r^2\omega^2\right)$
Elastic energy	$\frac{k}{2}\left(l_0 - r\right)^2$	$\frac{k}{2}\left(l_0 - r\right)^2$
Normalization	ω^2	g/l_0
Small compression	$\rho := (r - l_0)/l_0 \le 0, \rho \ll 1$	$\rho := (r - l_0)/l_0 \le 0, \rho \ll 1$
Small angle	$\phi \sim \frac{\pi}{2}$	$\phi \sim \frac{\pi}{2}$

References

Alexander, R.M., 1976. Mechanics of bipedal locomotion. In: Davies, P.S. (Ed.), Perspectives in Experimental Biology. Pergamon Press, Oxford, UK, pp. 493–504.
Alexander, R.M., 1981. The gaits of tetrapods: adaptations for stability and economy. In: Symposia of the Zoological Society of London. Vol. 48, pp. 269–287.
Alexander, R. McN, 1984. The gaits of bipedal and quadrupedal animals. Int. J. Robot. Res. 3 (2), 49–59.
Alexander, R.M., 1989. Optimization and gaits in the locomotion of vertebrates. Physiol. Rev. 69, 1199–1227.
Alexander, R.M., 2003a. Principles of Animal Locomotion. Princeton University Press, Princeton.
Alexander, R.M., 2003b. Modelling approaches in biomechanics. Philos. Trans. R. Soc. Lond. Ser. B Math. Phys. Eng. Sci. 358, 1429–1435.
Arslan, Ö., Saranli, U., Morgül, Ö., 2009. Reactive footstep planning for a planar spring mass hopper. In: Proc. IEEE/RSJ International Conference on Intelligent Robots and Systems. IROS, pp. 160–166.
Birn-Jeffery, A.V., Higham, T.E., 2014. The scaling of uphill and downhill locomotion in legged animals. Integr. Comp. Biol. 54, 1159–1172.
Birn-Jeffery, A.V., Hubicki, C.M., Blum, Y., Renjewski, D., Hurst, J.W., Daley, M.A., 2014. Don't break a leg: running birds from quail to ostrich prioritise leg safety and economy on uneven terrain. J. Exp. Biol. 217, 3786–3796.
Blickhan, R., 1989. The spring-mass model for running and hopping. J. Biomech. 22, 1217–1227.
Blickhan, R., Full, R.J., 1993. Similarity of multilegged locomotion: Bouncing like a monopode. J. Comp. Physiol. A 173, 509–517.
Cavagna, G.A., Heglund, N.C., Taylor, C.R., 1977. Mechanical work in terrestrial locomotion: two basic mechanisms for minimizing energy expenditure. Am. J. Physiol. 233, R243–R261.
Cavagna, G.A., Margaria, R., 1966. Mechanics of walking. J. Appl. Physiol. 21, 271–278.
Cavagna, G.A., Margaria, R., Saibene, F.P., 1963. External work in walking. J. Appl. Physiol. 18, 1–9.
Coleman, M.J., Chatterjee, A., Ruina, A., 1997. Motions of a rimless spoked wheel: a simple three-dimensional system with impacts. Dyn. Stab. Syst. 12, 139–159.
Coleman, M.J., Holmes, P., 1999. Motions and stability of a piecewise holonomic system: the discrete chaplygin sleigh. Regul. Chaotic Dyn. 4, 1–23.
Croft, J.L., Schroeder, R.T., Bertram, J.E.A., 2017. The goal of locomotion: Separating the fundamental task from the mechanisms that accomplish it. Psychon. Bull. Rev. 24, 1675–1685.
Delp, S., 2023. Mobilize center. https://mobilize.stanford.edu/. (Retrived 22 June 2023).
Dickinson, M.H., Farley, C.T., Full, R.J., Koehl, M.A., Kram, R., Lehman, S., 2000. How animals move: an integrative view. Science 288, 100–106.
Farley, C.T., Blickhan, R., Saito, J., Taylor, C.R., 1991. Hopping frequency in humans: A test of how springs set stride frequency in bouncing gaits. J. Appl. Physiol. 71, 2127–2132.
Farley, C.T., Glasheen, J., McMahon, T.A., 1993. Running springs: speed and animal size. J. Exp. Biol. 185, 71–86.
Foster, K.L., Collins, C.E., Higham, T.E., Garland, Jr., T., 2015. Determinants of lizard escape performance: decision, motivation, ability, and opportunity. In: Cooper, Jr., W.E., D.T., Blumstein (Eds.), Escaping from Predators: An Integrative View of Escape Decisions. Cambridge University Press, Cambridge, UK, pp. 287–321.
Foster, K.L., Selvitella, A.M., 2020. Learning the locomotion behaviour of lizards transfers across environments. In: International Conference on Machine Learning 2020 Workshop on Computational Biology. July 17th, 2020. https://icml-compbio.github.io/2020/papers/WCBICML2020_paper_2.pdf.
Foster, K.L., Selvitella, A.M., 2022a. Anolis ecomorph biomechanics across arboreal environments: What can machine learning tell us about behavioral plasticity in lizards? Integr. Comp. Biol. 62, S99.
Foster, K.L., Selvitella, A.M., 2022b. Transfer of anolis locomotor behavior across environments and species. Integr. Comp. Biol. 62 (3), 774–790.
Fukuchi, R.K., Fukuchi, C.A., Duarte, M., 2017. A public dataset of running biomechanics and the effects of running speed on lower extremity kinematics and kinetics. PeerJ 5, e3298, https://figshare.com/articles/dataset/A_comprehensive_public_data_set_of_running_biomechanics_and_the_effects_of_running_speed_on_lower_extremity_kinematics_and_kinetics/4543435.
Full, R.J., Koditschek, D.E., 1999. Templates and anchors: neuromechanical hypotheses of legged locomotion on land. J. Exp. Biol. 202, 3325–3332.
Garland, Jr., T., Losos, J.B., 1994. Ecological morphology of locomotor performance in squamate reptiles. In: Wainwright, P.C., Reilly, S.M. (Eds.), Ecological Morphology: Integrative Organismal Biology. University of Chicago Press, Chicago, USA, pp. 240–302.
Geyer, H., 2001. Movement Criterion of Fast Locomotion: Mathematical Analysis and Neuro-Biomechanical Interpretation with Functional Muscle Reflexes (Diploma thesis). Carnegie Mellon University, Pittsburgh, USA.
Geyer, H., 2005. Simple Models of Legged Locomotion Based on Compliant Limb Behavior (Ph.D. thesis). Friedrich-Schiller-Universität, Jena, Germany.
Geyer, H., Seyfarth, A., Blickhan, R., 2005. Spring-mass running: simple approximate solution and application to gait stability. J. Theoret. Biol. 232, 315–328.
Geyer, H., Seyfarth, A., Blickhan, R., 2006a. Compliant leg behaviour explains basic dynamics of walking and running. Proc. R. Soc. B: Biol. Sci. 273, 2861–2867.
Geyer, H., Seyfarth, A., Blickhan, R., 2006b. Positive force feedback in bouncing gaits? Proc. R. Soc. B: Biol. Sci. 270, 2173–2183.

Ghigliazza, R.M., Altendorfer, R., Holmes, P., Koditschek, D.E., 2003. A simply stabilized running model. SIAM J. Appl. Dyn. Syst. 2, 187–218.
Ghigliazza, R.M., Holmes, P., 2005. Towards a neuromechanical model for insect locomotion: Hybrid dynamical systems. Regul. Chaotic Dyn. 10, 193–225.
Goebel, R., Sanfelice, R.G., Teel, A.R., 2012. Hybrid Dynamic Systems: Modeling, Stability, and Robustness. Princeton University Press, Princeton.
Gordon, M.S., Blickhan, R., Dabiri, J.O., Videler, J.J., 2017. Animal Locomotion: Physical Principles and Adaptations, first ed. CRC Press, Boca Raton.
Holmes, P., Full, R.J., Koditschek, D., Guckenheimer, J., 2006. The dynamics of legged locomotion: Models, analyses, and challenges. SIAM Rev. 48, 207–304.
Hooren, B.Van., Fuller, J.T., Buckley, J.D., Miller, J.R., Sewell, K., Rao, G., Barton, C., Bishop, C., Willy, R.W., 2020. Is motorized treadmill running biomechanically comparable to overground running? A systematic review and meta-analysis of cross-over studies. Sports Med. 50 (4), 785–813.
Iida, F., Rummel, J., Seyfarth, A., 2008. Bipedal walking and running with spring-like biarticular muscles. J. Biomech. 41, 656–667.
Kilic, A.U., Braun, D.J., 2023. A novel approximation for the spring loaded inverted pendulum model of locomotion. In: 2023 IEEE/RSJ International Conference on Intelligent Robots and Systems. IROS, Detroit, MI, USA, pp. 4315–4321.
Margaria, R., 1976. Biomechanics and Energetics of Muscular Exercise. Clarendon Press, Oxford.
McGeer, T., 1990a. Passive bipedal running. Proc. R. Soc. B: Biol. Sci. 240, 107–134.
McGeer, T., 1990b. Passive dynamic walking. Int. J. Robot. Res. 9, 62–82.
McMahon, T.A., Cheng, G.C., 1990. The mechanism of running: how does stiffness couple with speed? J. Biomech. 23, 65–78.
Mochon, S., McMahon, T.A., 1980. Ballistic walking. J. Biomech. 13, 49–57.
Müller, R., Birn-Jeffery, A.V., Blum, Y., 2016. Human and avian running on uneven ground: a model-based comparison. J. R. Soc. Interface 13, 20160529.
Patek, S.N., Biewener, A.A., 2018. Animal Locomotion, second ed. Oxford University Press, Oxford.
Poulakakis, I., Grizzle, J.W., 2009. The spring loaded inverted pendulum as the hybrid zero dynamics of an asymmetric hopper. IEEE Trans. Autom. Control 54 (8), 1779–1793.
Raibert, M.H., 1986. Legged Robots that Balance. MIT Press, Cambridge.
Raibert, M., Blankespoor, K., Nelson, G., Playter, R., 2008. BigDog, the Rough-Terrain quadruped robot. IFAC Proc. Vol. 41, 10822–10825.
Ruina, A., 1998. Non-holonomic stability aspects of piecewise holonomic systems. Rep. Math. Phys. 42, 91–100.
Saranlı, U., Arslan, Ankaralı, M.M., Morgül, Ö., 2010. Approximate analytic solutions to non-symmetric stance trajectories of the passive spring-loaded inverted pendulum with damping. Nonlinear Dynam. 62, 729–742.
Saranli, U., Koditschek, D.E., 2003. Template based control of hexapedal running. In: Proceedings of the IEEE International Conference on Robotics and Automation. Taipei, Taiwan, pp. 1374–1379.
Schwind, W.J., 1998. Spring Loaded Inverted Pendulum Running: A Plant Model (Doctoral thesis). University of Michigan, Ann Arbor, MI, USA.
Schwind, W.J., Koditschek, D.E., 2000. Approximating the stance map of a 2-DOF monoped runner. J. Nonlinear Sci. 10, 533–568.
Seipel, J.E., Holmes, P., 2005. Running in three dimensions: Analysis of a point-mass Sprung-leg model. Int. J. Robot. Res. 24 (8), 657–674.
Selvitella, A.M., Foster, K.L., 2022a. Gait stability of the spring-mass model of planar locomotion on inclines. Integr. Comp. Biol. 62, S99.
Selvitella, A.M., Foster, K.L., 2022b. The spring-mass model and other reductionist models of bipedal locomotion on inclines. Integr. Comp. Biol. 62 (5), 1320–1334.
Selvitella, A.M., Foster, K.L., 2023. On the variability and dependence of human leg stiffness across strides during running and some consequences for the analysis of locomotion data. R. Soc. Open Sci. 10, 230597.
Seok, S., Wang, A., Chuah, M.Y., Otten, D., Lang, J., Kim, S., 2013. Design principles for highly efficient quadrupeds and implementation on the MIT Cheetah robot. In: 2013 IEEE International Conference on Robotics and Automation. pp. 3307–3312.
Seyfarth, A., Apel, T., Geyer, H., Blickhan, R., 2001. Limits of elastic leg operation. In: Blickhan, R. (Ed.), Motion Systems. Shaker Verlag, Aachen, Germany, pp. 102–107.
Seyfarth, A., Geyer, H., Günther, M., Blickhan, R., 2002. A movement criterion for running. J. Biomech. 35, 649–655.
Shahbazi, M., Babuška, R., Lopes, G.A.D., 2016. Unified modeling and control of walking and running on the spring-loaded inverted pendulum. IEEE Trans. Robot. 32 (5), 1178–1195.
Srinivasan, M., Ruina, A., 2005. Computer optimization of a minimal biped model discovers walking and running. Nature 439, 72–75.
Usherwood, J.R., 2005. Why not walk faster? Biol. Lett. 1, 338–341.
Usherwood, J.R., 2010. Inverted pendular running: a novel gait predicted by computer optimization is found between walk and run in birds. Biol. Lett. 6, 765–768.
Usherwood, J.R., 2016. Reductionist models of walking and running. In: Bertram, J.E.A. (Ed.), Understanding Mammalian Locomotion. (Chapter 6).
Usherwood, J.R., 2020. An extension to the collisional model of the energetic cost of support qualitatively explains trotting and the trot–canter transition. J. Exp. Zool. A 333 (1), 9–19.
Uyanık, I., Morgül, Ö., Saranlı, U., 2015. Experimental validation of a feed-forward predictor for the spring-loaded inverted pendulum template. IEEE Trans. Robot. 31 (2), 208–216.
van der Schaft, A., Schumacher, H., 2000. An Introduction to Hybrid Dynamical Systems. Springer, London.
Westervelt, E.R., Grizzle, J.W., Koditschek, D.E., 2003. Hybrid zero dynamics of planar bipedal walkers. IEEE Trans. Autom. Control 48 (1), 42–56.
Whittacker, E.T., 1904. A Treatise on the Analytical Dynamics of Particles and Rigid Bodies, fourth ed. Cambridge University Press, New York.
Yu, H., Gao, H., Deng, Z., 2021. Toward a unified approximate analytical representation for spatially running spring-loaded inverted pendulum model. IEEE Trans. Robot. 37 (2), 691–698.
Yu, H., Li, M., Cai, H., 2012. Approximating the stance map of the SLIP runner based on perturbation approach. In: 2012 IEEE International Conference on Robotics and Automation. Saint Paul, MN, pp. 4197–4203.